**TITLE**

# Spatial and temporal coordination of Duox/TrpA1/Dh31 and IMD pathways is required for the efficient elimination of pathogenic bacteria in the intestine of *Drosophila* larvae.

**Authors**

Fatima Tleiss[1], Martina Montanari[2], Olivier Pierre[1], Julien Royet[2]*, Dani Osman[3]*, Armel Gallet[1]* and C. Léopold Kurz[2]*

**affiliations**

1 : Université Côte d'Azur, CNRS, INRAE, ISA, France

2: Aix-Marseille Université, CNRS, IBDM, Marseille, France

3: UMR PIMIT (Processus Infectieux en Milieu Insulaire Tropical) CNRS 9192-INSERM 1187-IRD 249-Université de La Réunion, île de La Réunion, France.

* Corresponding authors: e-mail: armel.gallet@unice.fr; leopold.kurz@univ-amu.fr; dani.osman@univ-reunion.fr; julien.royet@univ-amu.fr

**Abstract**

Multiple gut antimicrobial mechanisms are coordinated in space and time to efficiently fight foodborne pathogens. In *Drosophila melanogaster*, production of reactive oxygen species (ROS) and antimicrobial peptides (AMPs) together with intestinal cell renewal play a key role in eliminating gut microbes. A complementary mechanism would be to isolate and treat pathogenic bacteria while allowing colonization by commensals. Using real-time imaging to follow the fate of ingested bacteria, we demonstrate that while commensal *Lactiplantibacillus plantarum* freely circulate within the intestinal lumen, pathogenic strains such as. *Erwinia carotovora* or *Bacillus thuringiensis*, are blocked in the anterior midgut where they are rapidly eliminated by antimicrobial peptides. This sequestration of pathogenic bacteria in the anterior midgut requires the Duox enzyme in enterocytes, and both TrpA1 and Dh31 in enteroendocrine cells. Supplementing larval food with hCGRP, the human homolog of Dh31, is sufficient to block the bacteria, suggesting the existence of a conserved mechanism. While the IMD pathway is essential for eliminating the trapped bacteria, it is dispensable for the blockage. Genetic manipulations impairing bacterial compartmentalization result in abnormal colonization of posterior midgut regions by pathogenic bacteria. Despite a functional IMD pathway, this ectopic colonization leads to bacterial proliferation and larval death, demonstrating the critical role of bacteria anterior sequestration in larval defense. Our study reveals a temporal orchestration during which pathogenic bacteria, but not innocuous, are confined in the anterior part of the midgut in which they are eliminated in an IMD pathway dependent manner.

## AUTHOR SUMMARY

Typically, when considering the immune response of animals to infection, we focus on classical immunity, encompassing both innate and adaptive aspects such as antimicrobials and circulating immune cells. However, a broader perspective on immunity includes additional strategies that enhance host protection, such as behavioral avoidance and internal mechanisms that restrict pathogen propagation. In our study using *Drosophila* larvae as a model, we uncovered spatially and temporally interconnected events that are crucial for effectively combating intestinal infections. Our findings reveal a two-step defense mechanism: first, the larvae rapidly discriminate between bacterial strains, effectively confining hazardous ones in the anterior section of the intestine. These blocked bacteria trigger the synthesis and release of antimicrobial peptides by the host, which ultimately eradicate the entrapped pathogens. Our experiments show that larvae capable of both limiting bacteria spreading and producing antimicrobial peptides withstand infections. In contrast, the absence of either one of these sequential defenses results in high mortality among the larvae, emphasizing the importance of each step and the necessity of their precise coordination in the immune response.

64 **INTRODUCTION**

65 One of the key avenues by which bacterial pathogens infiltrate a host is through the
66 ingestion of contaminated food. Following the entry of bacteria in the intestine, the host
67 defense mechanisms will operate in a temporal manner, with mechanical and
68 constitutive chemical barriers serving as the first line of defense, followed by inducible
69 mechanisms involving the production of reactive oxygen species (ROS), the
70 transcription, translation, and secretion of antimicrobial peptides (AMPs) as well as
71 inter-organ signaling to cope with possible upcoming stages of infection. This
72 temporality is evident between innate and adaptive immunity, with the former
73 considered the primary defense line that contains and combats the threat while
74 preparing the more subtle adaptive response.

75 To focus on deciphering innate immune processes, the insect *Drosophila*
76 *melanogaster* has been widely and successfully used (Neyen et al., 2014; Younes et
77 al., 2020). This model has made it possible to establish the chronology of the events
78 involved in the defense against pathogenic bacteria. In *Drosophila,* as in all
79 metazoans, a layer made of mucus, completed with a peritrophic membrane in insect
80 midguts, protects the intestine lining from direct contact with pathogens (Hegedus et
81 al., 2009; Lemaitre and Miguel-Aliaga, 2013; Pelaseyed et al., 2014). In adult
82 *Drosophila*, a conserved immune response involving the production of ROS by Duox
83 (Dual oxidase) enzyme in enterocytes is triggered in the intestine as early as 30
84 minutes after ingesting pathogenic bacteria. ROS directly damage bacterial
85 membranes (Benguettat et al., 2018; Ha et al., 2009; Ha et al., 2005; Lee et al., 2013)
86 but also exert an indirect effect in adults by triggering visceral spasms through the host
87 detection of ROS mediated by the TrpA1 nociceptor and subsequent secretion of

88 Diuretic Hormone 31 (Dh31) by enteroendocrine cells (Benguettat et al., 2018; Du et
89 al., 2016a). Dh31 then binds its receptor on visceral muscles, triggering contractions
90 that expedite bacterial elimination (Benguettat et al., 2018). This pathway seems to be
91 conserved during evolution as TrpA1 is a *Drosophila* homolog of TRP receptors that
92 respond to noxious conditions (Ogawa et al., 2016) and Dh31 is the *Drosophila*
93 homolog of the mammalian CGRP (Guo et al., 2021; Nässel and Zandawala, 2019).
94 In parallel, the IMD innate immune pathway is activated following bacterial
95 peptidoglycan detection, leading to the transcription of AMP encoding genes and to
96 the subsequent secretion of the peptides that kill bacteria (Capo et al., 2019).

97 Previous study has explored the dynamics of food transit involving intestinal
98 valves and Dh31 in the context of *Drosophila* larvae (LaJeunesse et al., 2010)
99 Additionally, the perturbed circulation of bacteria within the intestine has been
100 documented in the literature. However, the intricate interplay between the
101 sequestration of bacteria in specific gut regions and their subsequent elimination has
102 remained largely unexplored. In our study, we leveraged a novel real-time
103 experimental system designed specifically for *Drosophila* larvae, enabling us to
104 meticulously trace the journey and ultimate fate of pathogenic bacteria ingested
105 alongside food. This approach has allowed us to shed light on the complex
106 mechanisms underpinning bacterial management within the larval gut, contributing a
107 significant advancement to our understanding of host-pathogen interactions at the
108 intestinal level. We characterized a new mechanism implicated in the blockage and
109 elimination of pathogenic bacteria in the anterior part of the midgut. We demonstrated
110 that this confinement is regulated by the ROS/TrpA1/Dh31 axis. Our results delineate
111 a model in which bacterial trapping arises from ROS production in the intestinal lumen
112 in response to pathogenic bacteria. These ROS compounds interact with TrpA1 in

113 Dh31-expressing enteroendocrine cells located between the anterior and middle
114 midgut, leading to Dh31 secretion and subsequent bacterial compartmentalization,
115 suggesting the closure of a valve, a midgut junction structure proposed by
116 (LaJeunesse et al., 2010). Interestingly, we found that we can ectopically induce the
117 trapping of fluorescent particles or innocuous bacteria using human CGRP that
118 replaces Dh31. Our findings also highlight the central role of this blockage, which acts
119 first allowing sufficient time for the subsequent eradication of blocked pathogens by
120 the IMD pathway and its downstream effectors. Collectively, our data unravel a finely
121 tuned coordination between the ROS/TrpA1/Dh31 axis and the IMD pathway, enabling
122 an effective bactericidal action of AMPs.

123

124

125 **RESULTS**

126 **Bacterial confinement in the anterior part of larval intestine**

127 The translucency of *Drosophila* larvae allows for live studies of immune defense
128 components and their coordination in eradicating pathogenic bacteria. In our prior
129 work, we revealed a modified food transit in larvae exposed to the Gram-negative
130 opportunistic bacterium *Erwinia carotovora carotovora* (*Ecc15*), a process that
131 involved TrpA1 (Keita et al., 2017).

132 Using blue food dye, we tracked the presence of food in the intestinal lumen and
133 observed that larval guts were blue without bacterial contaminants, while in the
134 presence of *Ecc15*, they appeared clearer (Keita et al., 2017). Such a strategy was
135 already used to delineate whether oral infection by *Pseudomonas entomophila* could
136 modulate food transit (Liehl et al., 2006). However, our previous assay with *Ecc15*

137 was limited to 1h post-ingestion and using a food dye, not directly monitoring the fate
138 of the ingested bacteria over the time. We therefore designed a new protocol allowing
139 to film the fate of fluorescent bacteria once ingested by the larvae. Animals are fed for
140 1h with food contaminated with fluorescent bacteria to investigate the localization of
141 these pathogens within the intestinal tract. Following this feeding period, the animals
142 were transferred to a wet chamber devoid of food. This setup allowed us to monitor
143 the positional dynamics of the bacteria within the intestine over time, without further
144 food intake influencing the observations. We tested three different fluorescent
145 bacteria: *Ecc15-GFP* (*Ecc*), *Bacillus thuringiensis-GFP* (*Bt*, an opportunistic Gram-
146 positive bacterium) and *Lactiplantibacillus plantarum-GFP* (*Lp*, a commensal Gram-
147 positive bacterium). After 1 hour of feeding on contaminated media, *Ecc* and *Bt* were
148 concentrated in the anterior midgut (Movies 1 and 2). The location of the bacteria
149 specifically in the anterior part of the intestine following 1h exposure was confirmed
150 when individuals from populations were imaged and counted (Fig 1A). The
151 consistently defined limits of the area containing bacteria in the anterior part of the gut
152 across our observations strongly indicate the presence of a physical boundary. This
153 reproducibility contrasts with what would be expected if the cessation of food intake
154 were responsible for halting bacterial progression, which would likely result in more
155 variable bacterial distributions within the intestine among individual subjects (Fig 1A).
156 Remarkably, with animals fed 1h with *Ecc* or *Bt* and transferred in a wet chamber,
157 tracking the GFP signal over time revealed that it remained in the anterior part of the
158 larva and began to fade 6 hours after ingestion (Movies1 and 2; SUPP1A and
159 SUPP1B). This fading suggests the elimination of the bacteria, while the larva
160 continued to exhibit active movements. This pattern was observed for both *Ecc* and
161 *Bt*. However, unlike the opportunistic bacteria *Ecc* and *Bt*, a food mixture contaminated

162 with *Lp* led to the bacteria being present in the posterior compartment of the larval
163 midgut after 1 hour of feeding and remained there throughout the 16-hour duration of
164 our observation (Movie 3, Fig 1A and SUPP1C) (Storelli et al., 2018). To better
165 characterize the blockage phenomenon, we counted the ratio of larvae with trapped
166 GFP-bacteria 1h post feeding. Importantly, in all our experiments, approximately 20%
167 of larvae displayed an absence of fluorescent bacteria within the intestinal lumen.
168 Notably, this proportion remained consistent across different bacterial strains used to
169 contaminate the food, indicating that the specific compartmentalization of pathogenic
170 bacteria we observed is not related to a global food-intake cessation. Instead, these
171 findings suggest the deployment of a targeted sequestration mechanism. Focusing on
172 animals containing fluorescent bacteria, we found that more than 80% of the larvae
173 had *Ecc* and *Bt* bacteria localized in the anterior part of the midgut (Fig 1A and 1B).
174 The portion of the intestine containing the fluorescent bacteria is delimited posteriorly
175 by an extensive turn, a region that was suggested to act like a valve (LaJeunesse et
176 al., 2010). To confirm our findings, we dissected the intestines of larvae that had
177 ingested the bacteria. Our analysis confirmed that *Ecc* and *Bt* were predominantly
178 located in the anterior part of the intestines, whereas *Lp* was not, supporting our initial
179 observations (SUPP2A). Our data collectively indicate that pathogenic bacteria, such
180 as *Ecc* and *Bt*, are spatially confined to the anterior part of the larval midgut before
181 their disappearance. In contrast, the commensal bacterium *Lp* is distributed
182 throughout the midgut, persisting principally in the posterior part.

183 **The anterior intestinal confinement of pathogenic bacteria is dose-specific and**
184 **occurs rapidly**

185 We hypothesized that the bacterial localization specifically in the anterior part of the
186 larval intestine was an active host response and might be dependent on the bacterial
187 dose. To test this, we exposed larvae to varying concentrations of *Ecc* and *Bt* and
188 measured the blockage ratio. We found that a concentration of $2.10^9$ *Ecc* bacteria per
189 ml was sufficient to induce the bacterial compartmentalization, whereas for *Bt*, a
190 concentration of $4.10^{10}$ *Bt* bacteria per ml was required (Fig 2A).

191 For all subsequent experiments, we used $4.10^{10}$ bacteria per ml.

192 In previous contamination assays, we arbitrary used a 1-hour time point to
193 assess the phenotype. However, observations of bacterial blockage occurring within
194 minutes suggested that this response does not require *de novo* protein synthesis by
195 the host. Shorter exposure times revealed that *Ecc* was blocked in the anterior part of
196 the intestine within 15 minutes, while *Bt* showed a similar pattern beginning at 15
197 minutes and completing by 30 minutes (Fig 2B and 2C). Based on these results, we
198 defined 1h as our standard exposure time of larvae with bacterial contaminated food.

199 Our assays typically involved groups of approximately 50 larvae to observe
200 population-level phenomena. Recent studies have suggested that larval behavior can
201 be influenced by group dynamics (Dombrovski et al., 2019; Dombrovski et al., 2017;
202 Louis and de Polavieja, 2017; Mast et al., 2014). To determine whether group size
203 affects the bacterial confinement, we exposed groups of varying sizes to *Bt* or *Ecc* and
204 measured the blockage ratio. The phenomenon proved robust even with a single larva
205 exposed to contaminated food, indicating that the response was not influenced by
206 group size under our experimental conditions (Fig 2D). Based on these findings, for
207 all subsequent experiments, we standardized the conditions using $4.10^{10}$ bacteria per
208 ml, a 1-hour exposure time, and groups of at least 20 larvae.

209 **Host TrpA1 and Dh31 are crucial for the blockage phenotype**

210 In our previous study reporting an altered food transit for larvae exposed to a food
211 contaminated with *Ecc* (Keita et al., 2017), we identified the gene *TrpA1* as essential
212 for the host response. The TrpA1 protein, a member of the TRP channel family,
213 facilitates Ca2+ entry into cells at temperatures over 25°C or upon exposure to
214 chemicals such as ROS (Du et al., 2016b; Gu et al., 2019; Guntur et al., 2015). This
215 channel, involved in nociception (Lapointe and Altier, 2011), has been linked to
216 intestinal muscle activity in adult *Drosophila* following *Ecc* exposure (Du et al., 2016a)
217 and in response to ROS production by the host (Benguettat et al., 2018). We examined
218 the role of TrpA1 during the larval response to contaminated food using $TrpA1^{[1]}$
219 homozygous viable mutant in the experimental setup with fluorescent *Lp*, *Ecc* or *Bt*
220 bacteria. In these mutant larvae, while the localization of *Lp* in the posterior midgut
221 remained unchanged, *Ecc* and *Bt* were found in the posterior midgut. (Fig 3A, 3B,
222 movie 4 and SUPP3A). This observation underscores that TrpA1 is necessary for the
223 blockage of pathogenic bacteria in the anterior midgut and suggests that the
224 disappearance of the fluorescence observed for pathogenic bacteria within the
225 intestine of control animals may be due to bacteria being killed rather than fading of
226 GFP or plasmid loss. Considering previous reports on visceral contraction in adult
227 *Drosophila* linked to ROS production, detection by TrpA1, and Dh31 secretion to expel
228 bacteria (Benguettat et al., 2018; Du et al., 2016a), we wondered whether a similar
229 ROS/TrpA1/Dh31 signaling axis is necessary in larvae to block pathogenic bacteria in
230 the anterior midgut. Indeed, though the bacterial blockage we observed did not expel
231 microorganisms, it might involve muscle contractions related to the food
232 contamination. Thus, we tested the blockage ratio of $Dh31^{[KG09001]}$ homozygous viable
233 mutants ($Dh31^{-}$) exposed to *Lp*, *Bt* or *Ecc* bacteria. In contrast to control animals,

234 where fewer than 20% of larvae exhibited *Ecc* or *Bt* in the posterior section of the
235 intestine, for more than 60% of *Dh31*$^{-}$ mutant larvae, the pathogenic bacteria *Bt* or *Ecc*
236 were localized in the posterior midgut confirming Dh31's crucial role in this mechanism
237 (Fig 3A and 3B, movie 5 and SUPP3B). The localization of *Lp* was not affected (Fig
238 3B).

239 Given the possibility that the compartmentalization of pathogens we observed might
240 be driven by bacterial virulence factors, we aimed to further investigate the underlying
241 mechanism. To discern whether this phenomenon was specific to pathogenic bacteria
242 or could extend to non-pathogenic entities, we conducted experiments to determine if
243 abiotic particles or non-virulent bacteria could also be ectopically sequestered within
244 the gut. The human Calcitonin Gene-Related Peptide (hCGRP) is the functional
245 homolog of Dh31. Indeed, hCGRP has been shown to promote visceral muscle
246 contractions in adult flies (Benguettat et al., 2018). To investigate whether the bacterial
247 confinement could be triggered without pathogenic bacteria in response to a hormone,
248 we exposed larvae to either *Lp* or Dextran-FITC in the presence of hCGRP. While *Lp*
249 and Dextran-FITC were normally distributed throughout the midgut, adding hCGRP to
250 the food induced a significant blockage (Fig 3B and 3C and movie 6). This observation
251 implies that the confinement of bacteria within the gut is not solely a direct
252 consequence of pathogen toxicity. Intriguingly, despite the larvae being housed in a
253 wet chamber where no further food intake occurs (which could otherwise push the
254 bacteria towards the posterior gut), we noted that *Lp* initially sequestered in the
255 anterior midgut following the administration of hCGRP began to be released after 6
256 hours (movie 6 and SUPP3). This is suggestive of a dynamic and reversible
257 phenomenon, likely linked to Dh31/hCGRP hormone metabolization. This
258 demonstrates that the process could be triggered independently of the bacteria by a

259 hormone, independently of food-intake *per se*, highlighting it as an active host
260 mechanism that involves a specific portion of the gut capable of limiting the circulation
261 of the bacteria.

262 **Duox in Enterocytes and Dh31 in Pros+ cells control pathogenic bacteria**
263 **blockage**

264 The activation of TrpA1, potentially leading to the release of Dh31, ((Belinskaia et al.,
265 2023; Kondo et al., 2010; Kunst et al., 2014) could be a consequence of ROS
266 production in the host larval midgut in response to *Ecc* or *Bt*. The larval intestine
267 comprises two main cell populations: enterocytes (ECs) and enteroendocrine cells
268 (EECs). In adult *Drosophila*, Dh31 is stored in EECs and is secreted in response to
269 TrpA1 activation, a process well documented in literature (Benguettat et al., 2018;
270 Chen et al., 2016; Veenstra et al., 2008). The role of ROS in the immunity of adult
271 *Drosophila* intestine following infection has also been reported (Chakrabarti et al.,
272 2012; Ha et al., 2005; Lee et al., 2013; Ryu et al., 2006). To investigate the involvement
273 of ROS in the larval bacterial confinement, we focused on Duox, the primary enzyme
274 responsible for luminal ROS production. We spatially silenced *Duox* expression using
275 RNA interference (*UAS-Duox_IR*) driven by an ubiquitous driver (Da-Gal4), a driver
276 specific of ECs (Mex-Gal4) or Pros-Gal4, a construction driving expression in EECs
277 and subsets of neuroblasts. In parallel, using the same set of drivers, we tested the
278 effects of cell-autonomous *Dh31* silencing using RNAi (*UAS-Dh31_IR*). Upon
279 exposing these larvae to a food mixture contaminated with fluorescent *Ecc* or *Bt*, we
280 assessed the blockage ratio. Our results indicate that in larvae, Duox is essential in
281 ECs for the blockage of both *Ecc* and *Bt* (Fig 3D). Furthermore, silencing *Dh31* in
282 EECs not only confirmed the mutant phenotype but also indicated that Dh31,

283 necessary for the confinement, is required for the phenomenon in Pros+ cells. (Fig
284 3D). This data underscores the pivotal roles of Duox in ECs and Dh31 in Pros+ cells
285 for the entrapment of pathogenic bacteria in the anterior part of the *Drosophila* larval
286 midgut.

287 **Absence of ROS prevents blockage phenotype and leads to larval death**

288 Our data demonstrating that Duox protein is necessary for the confinement phenotype,
289 implies that ROS generated by this enzyme are critical. The involvement of TrpA1, a
290 known ROS sensor, further highlights the significance of these compounds in the
291 process. To corroborate the necessity of ROS, we neutralized luminal ROS using DTT
292 (Dithiothreitol), a potent reducing agent known for its efficacy against ROS, mixing it
293 with the larval food (Benguettat et al., 2018). In normal conditions, larvae fed with *Bt*
294 exhibit a compartmentalization of the bacteria in the anterior part of their intestine, as
295 shown previously in FIG 1A, 1B and Fig 4A. However, when the larvae were exposed
296 to a mixture of *Bt* and DTT, the intestinal sequestration of bacteria in the anterior
297 midgut was abolished (Fig 4A). The effect of DTT over the blockage phenotype was
298 quantified using DTT mixed to Dextran-FITC in order to compare with a condition
299 leading to an almost full posterior localization (FIG 4B). Together our results strongly
300 suggest that the role of Duox enzyme in producing ROS in the larval intestine is crucial,
301 and these ROS act as key signals initiating the confinement mechanism. ROS may be
302 produced to directly limit bacterial proliferation and meanwhile trigger a cascade of
303 events leading to sequestration in the anterior part.

304 **Blockage is crucial for bacterial elimination and larval survival**

305 Our real-time observations showed that between 6 and 8 hours after the bacterial
306 compartmentalization of *Bt* or *Ecc* in the anterior midgut, the bacteria disappeared

307 (movies 1 and movie 2, SUPP1A and SUPP1B). This led us to investigate the
308 relationship between pathogen localization and larval survival. The hypothesis was
309 that the disappearance of the GFP signal corresponded to the bacterial death. We
310 therefore assessed the *Lp*, *Bt* or *Ecc* load over time in dissected midguts of control
311 larvae previously exposed to contaminated food and then transferred to a wet chamber
312 without food. Consistent with our film data, while the *Lp* load remained stable, the
313 quantities of *Ecc* and *Bt* diminished rapidly in the intestines of control larvae, with no
314 bacteria detectable 8 hours post-ingestion and blockage (Fig 5A, 5B and 5C).
315 However, in the intestines of *TrpA1*$^{[1]}$ and *Dh31*$^{-}$ mutants, the amount of *Bt* and *Ecc*
316 increased overtime (Fig 5B and 5C). Interestingly, the quantity of bacteria present in
317 the intestine after a 1 hour feeding period was consistent across different host genetic
318 backgrounds for any given bacterial species. This uniformity highlights the process'
319 active regulation rather than attributing the observed patterns to a simple cessation of
320 food intake or a global disruption of peristalsis in *Dh31* and *TrpA1* mutants resulting in
321 a massive and uncontrolled influx of bacteria into the posterior part of the intestine.
322 Unfortunately, we were unable to assess the bacterial load beyond 6 hours due to the
323 deterioration of the midguts. Supporting this, in movies 4 and 5 (SUPP3A and
324 SUPP3B), we observed that *Bt* or *Ecc* bacteria which were not blocked in the anterior
325 part of the midgut did not disappear over time. More importantly, *TrpA1*$^{[1]}$ and *Dh31*$^{-}$
326 mutant larvae containing *Bt* or *Ecc* stopped to move suggesting they were dead. We
327 confirmed the precocious death of the *TrpA1*$^{[1]}$ and *Dh31*$^{-}$ larvae fed with either *Bt* or
328 *Ecc* compared to control animals (Fig 5D and 5E). Importantly, these mutants
329 exhibited sustained viability overnight in the wet chamber after having been fed 1h
330 with a mixture containing *Lp* or a bacteria-free diet (Fig 5E). Interestingly, control larvae
331 fed a mixture of *Bt* and DTT, which neutralizes ROS and thus inhibits the confinement,

332 also perished (Fig 5F). This mortality was not due to DTT, as larvae fed Dextran-FITC
333 plus DTT survived (FIG 5F). These findings suggest that, in larvae, the blockage of *Bt*
334 and *Ecc* in the anterior part of the midgut – involving a sequence of events with ROS
335 production by Duox, TrpA1 activation by ROS, and Dh31 secretion – is essential for
336 bacterial elimination by the host. Thus, failure to compartmentalize pathogenic
337 bacteria like *Ecc* or *Bt* results in their proliferation and consequent larval death.

338 **The confined area is delimited by TrpA1+/Dh31+ cells and muscular structures**

339 The above results suggest a working model involving the ROS/TrpA1/Dh31 axis in
340 which Dh31 release from EECs leads to muscle contractions. However, unlike in adult
341 *Drosophila*, where bacteria are expelled from the gut, in larvae, we observed a
342 blockage mechanism. To better understand the physiology of the process, we utilized
343 confocal microscopy to thoroughly examine larval midguts and explore the relationship
344 between TrpA1-positive (TrpA1+) cells, anterior confinement of the bacteria, and
345 muscular structures. In larval midguts, TrpA1+ cells were also Dh31+, and these
346 Dh31+ cells were identified as EECs (Pros+), typically located at the end of the anterior
347 midgut. With the reporter line we used (*TrpA1*-Gal4/UAS-RFP), we noted an average
348 of 3 TrpA1+/Dh31+ cells per gut (ranging from 2 to 6 cells across 14 examined guts,
349 see source data file) (Fig 6A-6F). This observation was in agreement with our genetic
350 and functional data linking Dh31 with Pros+ cells including EECs (FIG 3D) and
351 suggested that TrpA1 and Dh31 operate within the same cells (Fig 6C, 6C' and 6C'').
352 The shape of these TrpA1+ Dh31+ cells was characteristic of EECs (Fig 6A'). In
353 agreement with a model involving an interaction of secreted ROS with TrpA1 and a
354 subsequent local Dh31 release to act on muscles, following exposure to food
355 contaminated with fluorescent *Bt* or *Ecc*, the bacteria were confined in an area

356 delimited by the anterior part of the gut and the TrpA1+ cells patch (Fig 6B).
357 Additionally, we observed that the amount of Dh31 within Pros+ cells of larvae
358 confining bacteria was lower compared to those not exhibiting the blockage, such as
359 *TrpA1* mutant (Fig 6D and 6E). Then, we wondered whether specific muscle structures
360 would exist close to the TrpA1+ cells in the anterior midgut. Actin labeling revealed
361 fibrous structures on the basal side of the gut and attached to it in a transversal position
362 (Fig 6C'' and 6F-6H'). These structures, typically lost during dissection, have been
363 described previously, and the hypothesis of their connection with a valve at the junction
364 with the midgut was proposed in a report studying larval midgut peristalsis
365 (LaJeunesse et al., 2010). Notably, the attachment points of these filaments, or
366 tethers, corresponded with the locations of TrpA1+ cells and the boundary of the area
367 where *Ecc* or *Bt* were confined (Fig 6C'' and 6F-H). These filaments have been
368 described as longitudinal muscles emanating from two out of the four gastric caeca,
369 but this might be a misinterpretation of the images generated by Lajeunesse et al.
370 (2010). Indeed, a recent study describes these muscular structures using *in vivo*
371 observations without dissections. Interestingly, they show that these muscles belong
372 to a subgroup of alary muscles named TARMs (Thoracic Alary Related Muscles)
373 (Bataillé et al., 2020). Specifically, TARMsT1 connect the anterior of the larvae to the
374 extremities of gastric caeca, while TARMsT2 link the anterior part of the gut to the
375 larval epidermis. Our findings support the hypothesis that the observed muscular
376 structures close to the TrpA1+ cells are TARMsT2 (Fig 6C'', 6F-6H', SUPP 4 and
377 movie 7). These TARMsT2 are attached to the longitudinal gut muscles and the
378 intestine forms a loop at the attachment site (Fig 6H' and SUPP4) (Bataillé et al.,
379 2020). The presence of Dh31+ EECs in this specific curved region of the gut close to
380 the TARMsT2 attachment (Fig 6C") led to the hypothesis that this region may act like

381 a valve (LaJeunesse et al., 2010). Our genetic, functional and physiological data
382 confirm this model and reveal a new and crucial role in the context of pathogenic
383 bacteria ingestion.

384 **IMD pathway is mandatory for eliminating trapped bacteria**

385 In our study, we observed that control larvae were able to kill *Ecc* and *Bt* bacteria
386 trapped in the anterior part of the gut within 6-8 hours (movies 1 and 2 and Fig 5A-C).
387 This finding raised questions about the mechanism of bacterial elimination and the
388 potential role of the IMD (Immune Deficiency) pathway in this process. While larval
389 intestinal immunity is multifaceted, a key defense mechanism against bacteria is the
390 production and secretion of AMPs (Hanson and Lemaitre, 2020). Thus, we focused
391 our investigations on AMPs. Both *Ecc* and *Bt* possess DAP-type peptidoglycans
392 (PGN), known to activate the IMD signaling cascade, which leads to the production of
393 AMPs like Diptericin (Kaneko et al., 2006; Leulier et al., 2003; Stenbak et al., 2004).
394 We used various mutants deficient in components of the IMD pathway, including
395 PGRP-LC and PGRP-LE (PGN receptors), Dredd (an intracellular component), and
396 Relish (a NF-kB transcription factor) (Zhai et al., 2018). Additionally, we studied a
397 mutant, *ΔAMP14*, lacking 14 different AMPs (Carboni et al., 2022). We first assayed
398 whether the IMD pathway was required for the blockage phenotype upon ingestion of
399 *Bt* or *Ecc*. While *Lp* was distributed throughout the gut of IMD pathway mutants, *Ecc*
400 and *Bt* were confined to the anterior part of the intestine, akin to control larvae (movies
401 8-12, SUPP5 and SUPP6 and Fig 7A and 7B). Thus, the IMD pathway is not required
402 for the compartmentalization of *Ecc* and *Bt* in larval intestines. Nevertheless, the
403 movies suggested a death of the IMD mutant larvae despite the blockage of either *Bt*
404 or *Ecc*. We therefore tested the survival of these IMD pathway mutants following a 1h

405 feeding with a mixture containing or not (water) fluorescent bacteria followed by a
406 transfer into a humid chamber. While neither control animals nor the IMD pathway
407 mutants died following a 1h feeding period with a *Lp* contaminated or non-
408 contaminated food and transfer into a humid chamber, all the IMD pathway mutants,
409 including *ΔAMP14*, had a decreased survival after exposure to *Ecc* or *Bt* (Fig 7C and
410 7D). Thus, the IMD pathway is central for the survival of these animals with bacteria
411 blocked in the anterior part of the intestine. As this increased lethality in IMD pathway
412 mutants might be related to an uncontrolled growth of the confined *Bt* and *Ecc* bacteria,
413 we performed CFU counting. With *Bt* and *Ecc*, while the initial inoculum was divided
414 by $10^3$ in 8h in the control larvae, the bacterial population was maintained and even
415 increased 10-fold in IMD pathway mutants including *ΔAMP14* (Fig 7E and 7F).
416 Additional observations from filming the fate of *Bt* and *Ecc* in IMD pathway mutant
417 larvae confirmed these findings (movies 8-12). The GFP-bacteria, although
418 sequestered in the anterior part of the intestine, did not disappear, coinciding with
419 larval immobility and presumed death. In conclusion, our findings illustrate that
420 although the IMD pathway is dispensable for the initial compartmentalization of
421 pathogenic bacteria, a process contingent on the ROS/TrpA1/Dh31 axis, it plays a
422 crucial role in their subsequent elimination. Indeed, the AMPs produced following IMD
423 pathway activation are essential for killing the trapped bacteria and ensuring larval
424 survival (Figure 8).

425

426

427 **DISCUSSION**

428 Leveraging the transparency of the *Drosophila* larvae, we have successfully
429 developed a novel real-time experimental system to monitor the fate of fluorescent
430 bacteria ingested along with food. This methodological advancement has enabled us
431 to unveil a previously uncharacterized physiological pathway necessary for the
432 efficacy of the larval intestinal immune response. Our research has uncovered a
433 unique defense mechanism centered around the presumed valve located in the
434 anterior midgut, regulated by the enteroendocrine peptide Dh31 (LaJeunesse et al.,
435 2010). Notably, we observed that the pathogenic bacteria we tested, were confined to
436 the anterior section of the larval intestine as early as 15 minutes post-ingestion. We
437 determined that this intestinal sequestration of pathogenic bacteria necessitates a
438 ROS/TrpA1/Dh31 axis initiated by Duox activity in enterocytes in response to
439 pathogenic bacteria. We suspect the secreted ROS to interact with the TrpA1 ion
440 channel receptor located in Dh31-expressing enteroendocrine cells adjacent to the
441 valve-like structure (Figure 8). Previous studies on the interaction between ROS and
442 TrpA1 support our hypothesis (Ogawa et al., 2016). The confining of pathogenic
443 bacteria to the anterior part of the larval intestine is a mandatory step prior to their
444 subsequent elimination by the IMD pathway. Intriguingly, previous studies utilizing
445 fluorescent bacteria have already highlighted a specific localization of pathogenic
446 bacteria in the larval gut. Bacteria such as *Ecc15*, *Pseudomonas entomophila*,
447 *Yersinia pestis*, *Salmonella enterica serovar Typhimurium*, and *Shigella flexneri* were
448 observed predominantly in the anterior part of the larval gut 6 hours after oral infection
449 (Basset et al., 2000; Bosco-Drayon et al., 2012; Earl et al., 2015; Ramond et al., 2021;
450 Vodovar et al., 2005). Our findings suggest that these bacteria can all induce ROS
451 production by enterocytes, providing a unifying mechanism for their containment and

452 elimination in the larval gut. Interestingly, it has been reported that the opportunistic
453 pathogen *Staphylococcus aureus (strain USA300)* predominantly colonizes the
454 posterior midgut of *Drosophila* larvae, leading to the death of 93% of the larvae
455 (Ramond et al., 2021). This strain of *S. aureus* produces high levels of detoxifying
456 enzymes, such as catalase and superoxide dismutases, which effectively neutralize
457 ROS. The authors suggested that the neutralization of ROS bactericidal activity by
458 these enzymes is directly responsible for the bacterial proliferation and consequent
459 host mortality (Ramond et al., 2021). However, considering our findings, we propose
460 a complementary or an alternative interpretation: the neutralization of ROS by these
461 detoxifying enzymes might prevent the bacterial compartmentalization, thereby
462 allowing *S. aureus* to access and establish in the posterior midgut. Our data also
463 indicate that when pathogenic bacteria reach the posterior midgut, as observed in
464 larvae fed with DTT or in *TrpA1* or *Dh31* mutants, larval survival is significantly
465 jeopardized. This suggests that larval mortality could be attributed not to the inhibition
466 of ROS in the posterior midgut but rather to the presence of bacteria in this region. In
467 the study by Ramond et al. (2021) involving *S. aureus*, the observation of bacterial
468 spread into the posterior part was recorded 3 hours post-infection. It would be insightful
469 to further investigate the dynamics of bacterial diffusion to determine whether, like
470 other pathogens we studied, *S. aureus* is initially confined to the anterior part of the
471 gut shortly after ingestion, specifically around 15 minutes post-infection. This could
472 provide a broader understanding of the interplay between pathogen-specific strategies
473 and host defense mechanisms in *Drosophila* larvae.

474 Our study has focused on an elbow-shaped region in the *Drosophila* larval
475 midgut, characterized by a narrowing of the lumen and surrounded by muscular fibers.
476 This region, where we observed a halt in transit when food is contaminated, has been

477 aptly termed a valve due to its functional similarity to the human pyloric region.
478 Interestingly, LaJeunesse et al. (2010) reported the presence of muscular fibers in this
479 area while Bataillé et al. (2020) identified them as a subgroup of alary muscles known
480 as TARMs (Thoracic Alary Related Muscles). Specifically, TARMsT1 connect the
481 anterior part of the larvae to the extremities of a pair of gastric caeca, whereas
482 TARMsT2 link the anterior part of the intestine to the larval epidermis. Our actin
483 staining corroborates the identification of these muscles as TARMsT2, which are
484 attached to the longitudinal muscles of the intestine, causing the intestine to form a
485 loop at the site of attachment (Bataillé et al., 2020). The presence of Dh31-positive
486 enteroendocrine cells (EECs) in this specific elbow-shaped region, close to the
487 TARMsT2 attachment point, combined with our genetic and functional data, supports
488 the hypothesis that this region could exhibit a valve-like activity. This activity is likely
489 triggered by Dh31 or human Calcitonin Gene-Related Peptide (hCGRP) following
490 bacterial exposure. Notably, our previous research in adult *Drosophila* showed that
491 Dh31/hCGRP secretion by EECs induces contractions of the visceral longitudinal
492 muscle fibers, expelling pathogenic bacteria rapidly (Benguettat et al., 2018).
493 However, in larvae, while Dh31/hCGRP likely induces muscle contractions, the
494 ensuing action may manifest as the closure of the midgut junction, as evidenced by
495 the observed retention of pathogenic bacteria. Importantly, in both larvae and adults,
496 the same pathway and type of muscle fibers appear to be involved, as TARMsT2 are
497 connected to longitudinal fibers (Figure 6H') (LaJeunesse et al., 2010). This finding is
498 significant as it illustrates a conserved mechanism across developmental stages,
499 albeit with different outcomes: expulsion of pathogens in adults and containment in
500 larvae. In both cases, the overarching objective is the effective elimination of

501 pathogens, demonstrating the versatility and adaptability of the *Drosophila* immune
502 response.

503 Hence, our work shed lights on a yet to be anatomically characterized valve
504 structure within the *Drosophila* larval gut, presenting a potential model for studying the
505 functions and roles of mammalian pylori. Notably, CGRP (Calcitonin Gene-Related
506 Peptide) secreting enteroendocrine cells have been identified in the mammalian
507 pylorus, as highlighted in research by (Kasacka, 2009) and (Bulc et al., 2018). Drawing
508 parallels with mammalian stomachs, the pylorus is typically closed, opening only when
509 the stomach becomes full. In exploring the functionality of the *Drosophila* valve we
510 studied, we considered two hypotheses: one, where it operates similarly to its
511 mammalian counterpart, closing by default and opening in response to a full stomach,
512 and another, where it remains open by default and closes upon detection of infected
513 food in the intestine. Our observations with the commensal bacteria *Lp* (movie 3)
514 suggest an initial closure of the pylorus as food accumulates in the anterior part of the
515 intestine, followed by its opening to allow the passage of non-pathogen-contaminated
516 food. This indicates a dynamic and responsive mechanism in the *Drosophila* gut. In
517 contrast, when *Drosophila* larvae encounter food contaminated with pathogenic
518 bacteria, the valve seems to contract, effectively blocking the passage of contaminated
519 food into the anterior part of the intestine. This finding is significant as it not only
520 reveals a unique physiological response in *Drosophila* larvae but also provides a basis
521 for comparative studies with the mammalian gastrointestinal system, particularly in
522 understanding the regulatory mechanisms governing pyloric function.

523 An intriguing question is why animals without a functional IMD pathway die from
524 *Ecc* or *Bt* exposure while ROS production is still operating? Indeed, when the IMD

525 pathway is disabled, bacteria are still confined in the anterior part of the gut, but are
526 not effectively eliminated, resulting in larval death. This outcome strongly suggests
527 that ROS alone are insufficient for bacterial eradication, even though they have been
528 shown to damage and inhibit bacterial proliferation (Benguettat et al., 2018; Ha et al.,
529 2005). However, the role of ROS in the immune response remains crucial since their
530 timing of expression before antimicrobial peptides is likely a key factor for the efficiency
531 of the immune response. Our findings, together with those from other studies, highlight
532 the critical role of AMPs in fighting off virulent intestinal bacteria, particularly in
533 scenarios where ROS activity is compromised or inadequate (Ramond et al., 2021;
534 Ryu et al., 2006). Our findings emphasize the critical role of the ROS/TrpA1/Dh31 axis
535 in effectively eradicating ingested pathogens. The rapid production of ROS following
536 bacterial ingestion plays a pivotal role in closing the valve and retaining virulent
537 bacteria in the anterior midgut. Notably, this process does not necessitate a
538 transcriptional/translation response. In contrast, the production of antimicrobial
539 peptides is a lengthier process, involving the transcriptional activation of *AMP* genes
540 downstream of the IMD pathway, followed by their translation and secretion. The initial
541 confinement of bacteria in the anterior midgut allows time for AMPs to be produced to
542 eliminate the trapped bacteria, which is crucial for the organismal survival. This
543 anterior bacterial blockage is important since when virulent bacteria reach the
544 posterior midgut (in absence of ROS or in *TrpA1* or *Dh31* mutants) the larvae die
545 despite a functional IMD pathway. A key question arises: Is the posterior midgut less
546 equipped to combat bacteria? Research by (Bosco-Drayon et al., 2012) suggests that
547 while the posterior midgut can produce AMPs, this portion of the gut is predominantly
548 dedicated to dampening the immune response, particularly through the production of
549 amidases. This permits an immune tolerance likely fostering the establishment of the

550 commensal flora. Consistent with this, we observed that commensal bacteria like *Lp*
551 transit from the anterior to the posterior midgut and persist there without compromising
552 larval survival. Additionally, *Lp* inherent resistance to AMPs (Arias-Rojas et al., 2023)
553 further underscores the idea that the anterior midgut serves as a checkpoint where
554 certain bacteria are detained and eliminated, while others, like *Lp*, are permitted to
555 pass through. When the compartmentalization mechanism is compromised,
556 pathogens or pathobionts can spread into the posterior midgut, potentially eliciting an
557 inadequate dampened immune response. Thus, the anterior midgut acts as a critical
558 juncture in determining the fate of ingested bacteria, either leading to their elimination
559 or allowing their passage to the posterior midgut, where a more tolerant immune
560 environment prevails.

561 Understanding the practical application of this defense mechanism in the natural
562 environment of *Drosophila melanogaster* larvae is crucial. In the wild, *Drosophila*
563 adults are typically drawn to rotting fruits on which they lay eggs, exposing them and
564 their progeny to a plethora of fungi and bacteria. Consequently, developing larvae feed
565 and grow in these non-sterile conditions. In such environments, encountering
566 pathogenic microbes is inevitable. Evasion or avoidance behavior has been
567 documented as a potential strategy for dealing with pathogens (Surendran et al.,
568 2017). This behavior might enable larvae to seek environments that will supposedly
569 better sustain their survival. However, given the larvae constant consumption of their
570 surrounding media in a race to reach pupation, ingestion of pathogen-contaminated
571 food is a common risk. Under these circumstances, larvae have limited options prior
572 to the activation of their innate immune response. Discriminating innocuous from
573 potentially deleterious bacteria and then limiting the transit of the latter ones for
574 subsequent elimination by AMPs, clearly benefits the host. Nonetheless, the

575 effectiveness of this blockage strategy would be maximized if it were coordinated with
576 evasion behaviors. Such coordination could prevent repeated engagement in this
577 energy-intensive immune response, thus optimizing the larvae chances of reaching
578 pupation successfully. This interplay between immune response and behavioral
579 adaptation underlines the sophisticated strategies employed by *Drosophila* larvae to
580 navigate their microbial-rich environment.

581

582

583 **MATERIALS AND METHODS**

584 **1-Bacterial strain**

585 We used the following strains: *Bacillus-thuringiensis*-GFP (*Bt*) (Hachfi et al., 2023) (the
586 original strain, 4D22, is from the Bacillus Genetics Stock Center - www.bgsc.org),
587 *Erwinia carotovora* subsp. *carotovora*-GFP *15* (*Ecc*) (Basset et al., 2000) and
588 *Lactiplantibacillus plantarum*-GFP (*Lp*) (gift from Renata Matos and François Leulier)
589 (Storelli et al., 2018). *Bt* and *Ecc* were grown on standard LB agar plates at 30°C and
590 *Lp* was grown in MRS medium in anaerobic conditions at 37°C for at least 18 hours.

591 The solid medium used in our experiments was supplemented with antibiotics to
592 ensure the selective growth of our bacterial strains as follows: *Ecc*: Spectinomycin at
593 100µg/ml; *Bt*: Erythromycin at 10µg/ml; *Lp*: Chloramphenicol at 10µg/ml. Each
594 bacterium was plated from glycerol stocks for each experiment. A single colony was
595 used to prepare liquid cultures. Bacteria were inoculated in 500 ml of appropriate
596 medium containing antibiotics as follows *Ecc*: Spectinomycin at 100 µg/ml; *Bt*:
597 Erythromycin at 10µg/ml; *Lp*: Chloramphenicol at 10µg/ml. After overnight growth, the

598 cultures were centrifuged for 15 min at 7500 rpm. Bacterial infectious doses were
599 adjusted by measuring culture turbidity at an optical density of 600 nm. $OD_{600}$=100 for
600 *Lp* and *Ecc* corresponds to $4.9.10^7$CFU/µl. $OD_{600}$=100 for *Bt* corresponds to
601 $1,5.10^7$CFU/µl.

602 **2-FLY Stocks**

603 Flies were maintained at 25 °C on our standard fly medium (Nawrot-Esposito et al.,
604 2020) with12:12 light/dark cycle. Fly stocks used in this study and their origins are as
605 follows: Canton S (Bloomington #64349, the reference to compare with mutants and
606 noted as control), *TrpA1*$^{1}$ (Bloomington #26504), *Dh31*$^{KG09001}$ (Bloomington #16474),
607 *Dh31-Gal4* (Bloomington #51988), *PGRP-LC*$^{\Delta E}$ (Bloomington #55713), *PGRP-LE*$^{112}$
608 (Bloomington #33055), *Dredd*$^{F64}$ (Gift from B. Charroux), *Relish*$^{E20}$ (Bloomington
609 #55714), *ΔAMP14* (Gift from B. Lemaitre; (Carboni et al., 2022)), *TrpA1*-Gal4/UAS-
610 RFP (Gal4 is Bloomington #527593, UAS is Bloomington #27392), *Da*-Gal4
611 (Bloomington #55851), *Pros*-Gal4 (gift form B. Charroux), *Mex*-Gal4 (gift from B.
612 Charroux), UAS-*Duox _IR* (Bloomington #38907), UAS-*Dh31_IR*
613 (Bloomington#25925).

614 **3-Infection experiments**

615 Oral infections were performed on mid-L3 larvae (3.5 days after egg laying). For each
616 experiment, between 20 and 50 non-wandering L3 larvae raised at 25°C were
617 collected and washed in PBS (1x). Bacterial pellets with starting OD 600nm ranging
618 from 300 to 400 were aligned with PBS1x at twice the desired final concentration.
619 Then, they were mixed 1:1 with yeast 40% in PBS (1x) and 500 µl of the infected food
620 were added at the bottom of an empty plastic fly vial (VWR) before adding the larvae
621 and sealing it with Parafilm. Then, the larvae were placed at 25°C in the dark. After 60

622 min, the larvae were washed in PBS (1x) and then counted for the presence of GFP-
623 bacteria or for other analyses.

624 **4-Larvae dissection**

625 After 60 min, the infected larvae were washed in PBS (1x). Guts were dissected and
626 fixed in formaldehyde 4% for 45 min, then washed twice in PBS (1x) for 10 min. Guts
627 were mounted between poly-L-lysine (SIGMA P8920-100ML) coated slides and
628 coverslips in Vectashield/DAPI (Vector Laboratories).

629 **5- Colony-forming unit (CFU) counting**

630 Following the established protocol for infection experiments, animals were exposed to
631 contaminated food for 1 hour. Subsequently, animals that had ingested bacteria were
632 either immediately processed for the initial time-point analysis or transferred to a wet
633 chamber for assessment at subsequent time-points. Importantly, since there was no
634 further exposure to contaminated food beyond the 1-hour treatment period, the CFU
635 assays we conducted measured the changes in the initial bacterial load within the
636 larvae over time. Infected animals were washed in ethanol 70% for 30s then rinsed in
637 PBS (1x). Guts were dissected in PBS (1x) and homogenized with a micropestle in
638 200 µl of LB medium. Samples were serially diluted in LB medium and plated on LB
639 agar plates overnight at 30°C. The Colonies Forming Unit (CFU) were counted the
640 following day. CFU counting has been performed at 5 time points: 1h, 2h, 4h, 6h and
641 8h after a 60 min intoxication (at least 20 larvae per point and 3 independent repeats).

642 **6-Mortality test**

643 Oral infection of the larvae was performed as described above in *Infection*
644 *experiments*. Larvae of the different genotypes fed 1h with *Bt*, *Lp* or *Ecc* were quickly

645 washed in 70% ethanol and then PBS (1x). Only the larvae that have eaten (containing
646 GFP bacteria in their intestine) were selected and put in a wet chamber for 18h at
647 25°C. Mortality was evaluated at this time-point.

648 **7- DTT and CGRP feeding**

649 Oral infection of the larvae was performed as described above in *Infection*
650 *experiments*.

651 **DTT:** DTT was added to the food at a final concentration of 100 nM and larvae were
652 fed during 60 min.

653 **hCGRP:** hCGRP (Sigma #C0167) was resuspended in distilled water. Larvae were
654 fed 1h as described above with a final hCGRP concentration of 400 µg/ml.

655 **8-Immunostaining**

656 Dissected intestines were washed twice with PBS (1x)-0.1% Triton X100 then
657 incubated for 3h in the blocking solution (10% of fetal calf serum, 0.1% Triton X100,
658 PBS (1x)). The blocking solution was removed and the primary antibodies added and
659 incubated overnight à 4°C in blocking solution. The following antibodies were used:
660 mouse anti-Prospero (MR1A-c, Developmental Studies Hybridoma Bank (DSHB)) at
661 1:200 and rabbit anti-Dh31 (gift from Jan Veenstra and Michael Nitabach; (Kunst et
662 al., 2014; Park et al., 2008) at 1:500. Secondary antibodies used were anti-mouse
663 Alexa647 (Invitrogen Cat# A-21235), anti-rabbit Alexa546 (Invitrogen Cat# A-11010).
664 All secondary antibodies were used at 1:1000. Guts were mounted in Fluoroshield-
665 DAPI mounting medium (Sigma F6057). Observations of GFP producing bacteria and
666 of TRPA1+ cells were done using the native fluorescence without immunostaining.

667 **9-RNAi experiments**

668 All the tested animals were F1 obtained from a cross between parents possessing the
669 Gal4 transgene and parents possessing the UAS-RNAi construction or from crosses
670 between w- animals (genetic background of the Gal4 and UAS lines) and a transgenic
671 line to serve as ctrl. The larvae were then fed with contaminated food as described
672 above.

673 **10-Images and movie acquisition**

674 Images acquisition was performed at the microscopy platform of the Institut Sophia
675 Agrobiotech (INRAE 1355-UCA-CNRS 7254-Sophia Antipolis) with the macroscope
676 Zeiss AxioZoom V16 with an Apotome 2 or a Zeiss Axioplan Z1 with Apotome 2
677 microscope. Images were analyzed using ZEN and Photoshop softwares. Movie
678 acquisitions were performed with the macroscope Zeiss AxioZoom V16 equipped with
679 the Hamamatsu Flash 4LT Camera. Larvae were captured every 5 minutes. Dead
680 larva images were acquired with a numeric Keyence VHX 2000 microscope.

681 **11-Data representation and statistical analyses**

682 The Graphpad Prism 8 software was used for statistical analyses.

683 CFU data analysis: the D'Agostino–Pearson test to assay whether the values are
684 distributed normally was applied. As not all the data sets were considered normal, non-
685 parametric statistical analysis such as non-parametric unpaired Mann–Whitney two-
686 tailed tests was used for all the data presented.

687 Blockage ratio and survival ratio datasets: as the values obtained from one larva are
688 categorical data with a *Yes* or *No* value, we used the two-sided Fisher exact t-test and

689 the 95% confidence interval to test the statistical significance of a possible difference
690 between a test sample and the related control.

691 For all the quantitative assays, at least 3 independent experiments were performed
692 and some were done in two different laboratories by more than one experimenter. The
693 results from all the experiments were gathered and the total amount of larvae tested
694 is indicated in the source data file. In addition, we do not show the average response
695 from one experiment representative of the different biological replicates, but an
696 average from all the data generated during the independent experiments in one graph.

697 **12-Source data files: detailed lines, conditions and statistics for the figure**
698 **section**

699 A file containing raw data, all the details about the experiments including the replicates,
700 sample size, genotypes and detailed statistical analyzes is available

701 https://figshare.com/articles/dataset/Tleiss_et_al_lockdown_Source_Data_File/2501
702 8352
703 DOI: 10.6084/m9.figshare.25018352
704

705 **FIGURE LEGENDS**

706 **FIGURE 1**

707 **Contrary to *Lp*, *Ecc* or *Bt* bacteria are found exclusively in the anterior part of**
708 **the gut.**

709 **A**: Pictures to illustrate the position of the green fluorescence of control L3 stage larvae
710 as a group (upper panel) or individual (lower panel) after having been fed 1h with a
711 media containing yeast and GFP-producing bacteria (*Ecc* or *Bt* or *Lp*). The white
712 asterisk indicates the anterior part of the animal. The white arrow indicates the
713 posterior limit of the area containing the fluorescent bacteria. Below the pictures are
714 schematics representing larvae, their gut, and the relative position of the GFP-
715 producing bacteria in green. Scale bar is 1mm.

716 **B**: Graphic representing the blockage ratio for L3 larvae exposed during 1h to a
717 mixture composed of yeast and fluorescent bacteria. The ratio of control larvae with a
718 distinguishable green fluorescence only in the upper part of the intestine, considered
719 as blocked bacteria, is represented. The ratio is calculated as: x larvae with bacteria
720 exclusively in the anterior part of the gut / (x larvae with bacteria exclusively in the
721 anterior part of the gut + y larvae with bacteria all along the gut). Larvae with no
722 distinguishable fluorescence were considered as non-eaters and discarded from the
723 quantifications. The ratio of larvae with no distinguishable fluorescence was not
724 influenced by the different conditions we tested. Shown is the average blockage ratio
725 with a 95% confidence interval from at least 3 independent assays with at least 30
726 animals per condition and trial. **** indicates p<0,0001, Fisher exact t-test. See the
727 source data file for details.

728 **FIGURE 2**

729 **Bacterial blockage is dose-dependent, occurs in less than 30 minutes, and does**
730 **not involve a group effect.**

731 **A**: Blockage ratio for control L3 larvae fed 1h with a mixture combining yeast with
732 different concentrations of fluorescent *Ecc* or *Bt*, concentrations are in number of
733 bacteria per ml. Shown is the average blockage ratio with a 95% confidence interval
734 from at least 3 independent assays with at least 18 animals per condition and trial. ****
735 indicates p<0,0001, Fisher exact t-test. See the source data file for details.

736 **B**: Representative images of control larvae fed during 30 min. with *Bt*. Scale bar is
737 1mm.

738 **C**: Blockage ratio for control L3 larvae fed during various times with a mixture
739 combining yeast with *Ecc* or *Bt.* Shown is the average blockage ratio with a 95%
740 confidence interval from at least 3 independent assays with at least 20 animals per
741 condition and trial. ns indicates values with differences not statistically significant, ****
742 indicates p<0,0001, Fisher exact t-test. See the source data file for details.

743 **D**: Blockage ratio for control L3 larvae fed 1h as individual animals or as groups of 10
744 or >40 with a mixture combining yeast with a constant concentration of *Ecc* or *Bt*
745 ($4.10^{10}$ bacteria per ml). Shown is the average blockage ratio with a 95% confidence
746 interval from at least 3 independent assays with the exact number of animals indicated
747 per condition and trial. ns indicates values with differences not statistically significant,
748 Fischer exact t-test. See the source data file for details.

749

750 **FIGURE 3**

751 **The bacterial blockage necessitates Duox in enterocytes, the TrpA1 channel and**
752 **Dh31 in Pros+ cells.**

753 **A**: Pictures to illustrate the localization of the fluorescent bacteria within the intestine
754 of control (ctrl), *Trpa1*$^{[1]}$ or *Dh31*$^{-}$ L3 larvae after having been fed 1h with a mixture of
755 yeast and *Ecc*. Scale bar is 1mm.

756 **B**: Blockage ratio for control (ctrl) L3 larvae or mutants for *Trpa1*$^{[1]}$ or *Dh31*$^{-}$ fed 1h with
757 a mixture combining yeast and *Lp* or *Ecc* or *Bt* or fluorescent Dextran with or without
758 hCGRP hormone. Shown is the average blockage ratio with a 95% confidence interval
759 from at least 3 independent assays with at least 30 animals per condition and trial. 0
760 indicates an absence of blockage. **** indicates p<0,0001, Fisher exact t-test. See the
761 source data file for details.

762 **C**: Pictures to illustrate the localization of the fluorescence within the intestine of control
763 L3 larvae after having been fed 1h with a mixture of yeast and fluorescent Dextran
764 with or without hCGRP hormone. Below the pictures are schematics representing
765 larvae, their gut, and the relative position of the fluorescence in green. Scale bar is
766 1mm.

767 **D**: Blockage ratio for animals expressing RNA interference constructions directed
768 against *Duox* mRNA or *Dh31* mRNA, ubiquitously (Da-Gal4), in enterocytes (Mex-
769 Gal4) or in enteroendocrine cells (Pros-Gal4) and then fed 1h with a mixture combining
770 yeast and *Ecc* or *Bt*. Shown is the average blockage ratio with a 95% confidence
771 interval from at least 3 independent assays with at least 30 animals per condition and

772 trial. ns indicates values with differences not statistically significant, **** indicates

773 p<0,0001 , Fisher exact t-test. See the source data file for details.

774

775 **FIGURE 4**

776 **Blocking the ROS with DTT prevents the compartmentalization of *Bt,* and the**
777 **larvae with bacteria in the posterior part of the intestine die.**

778 **A**: Pictures to illustrate the localization of the fluorescence within the intestine of
779 control (ctrl) L3 larvae after having been fed 1h with a mixture of yeast and *Bt* with or
780 without DTT. Below the pictures are schematics representing larvae, their gut, and
781 the relative position of the fluorescent bacteria in green. Scale bar is 1mm.

782 **B**: Blockage ratio for control (ctrl) L3 larvae fed 1h with a mixture combining yeast,
783 DTT and fluorescent Dextran or *Bt*. Shown is the average blockage ratio with a 95%
784 confidence interval from at least 3 independent assays with at least 18 animals per
785 condition and trial. ns indicates values with differences not statistically significant,
786 Fisher exact t-test. See the source data file for details.

787

788

789

790 **FIGURE 5**

791 **In the absence of blockage in *TrpA1*[1] or *Dh31*⁻ mutants, *Bt* and *Ecc* proliferate**
792 **in the larval intestine and the larvae die.**

793 **A**, **B** and **C**: quantification over time of the amount of *Lp*, (A), *Bt* (B) or *Ecc* (C) live
794 bacteria within the larval intestine of control (ctrl) (A, B and C), *Dh31*⁻ (B and C) and
795 *TrpA1*[1] (B and C) animals following a 1h feeding period with a solution containing
796 yeast and bacteria. CFU stands for Colony Forming Units. Shown is the average ±
797 SEM of at least 3 independent experiments with at least 7 guts each. After 8h, either
798 all the *TrpA1*[1] or *Dh31*⁻ larvae were dead or the intestines were severely damaged
799 preventing the CFU counting. * Indicates p<0,05, Mann Whitney, two-tailed test. See
800 the source data file for details.

801 **D**: Pictures of control (ctrl) or *TrpA1*[1] or *Dh31*⁻ larvae after 8h in a wet chamber
802 following a 1h feeding with a mixture of yeast and *Bt.* For control larvae, some animals
803 made pupae that are visible while for *TrpA1*[1] and *Dh31*⁻mutants, the dark larvae are
804 dead non-moving melanized animals. Scale bar is 1mm.

805 **E**: Ratio of dead control or T*rpA1*[1] or *Dh31*⁻ larvae after 8h in a wet chamber following
806 or not (water) a 1h feeding period with yeast mixed with *Lp* or *Ecc* or *Bt.* Shown is the
807 average with 95% confidence interval of at least 3 independent experiments with at
808 least 21 larvae per trial and condition. The 0 symbol indicates an absence of lethality.
809 **** indicates p<0,0001, Fisher exact t-test. See the source data file for details.

810 **F**: Ratio of dead control (ctrl) larvae after 8h in a wet chamber following a 1h feeding
811 period with a mixture combining yeast, DTT and Dextran fluorescent beads or *Bt*.
812 Shown is the average with 95% confidence interval of at least 3 independent

813 experiments with at least 18 larvae per trial and condition. The 0 symbol indicates an
814 absence of lethality. **** indicates p<0,0001, Fisher exact t-test. See the source data
815 file for details.
816

817

818 **FIGURE 6**

819 **TrpA1+ cells in the gut are enteroendocrine cells concentrated in a portion of**
820 **the intestine bordering the blocked bacteria.**

821 Confocal fluorescent pictures of the anterior portions of L3 larval intestines to detect;
822 longitudinal and transversal muscles concentrated in actin (F, G, H and H'), TrpA1+
823 cells producing RFP (A, A', B, C, C'' and F), GFP-bacteria (B, G and H), Dh31+ cells
824 (C', C'', D and E), Pros+ cells (D and E) and nuclei with DNA staining (A, A', B, C'', D,
825 E and G).

826 In B, D, E, G, H and H'; animals were previously fed for 1h with a mixture containing
827 bacteria and yeast with *Bt* (B, D and E) or *Ecc* (G, H and H'). When present, the white
828 star indicates the anterior part of the intestinal portion shown, the arrows point to
829 TARMs and the > symbols point to TrpA1+ cells. The empty squares in A and H with
830 dashed lines correspond to the portion of the image magnified in A' and H',
831 respectively. Scale bar in A, B, F, G and H represents 500µm, in A', C, D, E and H'
832 represents 100 µm.

833

834

835

836 **FIGURE 7**

837 **IMD pathway is not required for the blockage but essential for larvae survival**
838 **and *Bt* or *Ecc* clearance.**

839 **A**: Pictures to illustrate the localization of the fluorescence within the intestine of
840 *PGRP-LC*$^{[\Delta E]}$ L3 larvae after having been fed 1h with a mixture of *Lp* or *Ecc* or *Bt*.
841 Scale bar is 1mm.

842 **B**: Blockage ratio for control L3 larvae or mutants of the IMD pathway fed 1h with a
843 mixture combining yeast and *Lp* or *Ecc* or *Bt*. Shown is the average with 95%
844 confidence interval of at least 3 independent experiments with at least 20 larvae per
845 trial and condition. ns indicates values with differences not statistically significant,
846 Fisher exact t-test. See the source data file for details.

847 **C**: Pictures of *PGRP-LC*$^{[\Delta E]}$, *Rel*$^{[E20]}$ or *ΔAMP14* mutant larvae after 18h in a wet
848 chamber following a 1h feeding with a mixture of yeast and *Bt*. The dark larvae are
849 dead non-moving melanized animals. *ΔAMP14* is a mutant deleted for 14
850 antimicrobial-encoding genes.

851 **D**: Ratio of dead control or *TrpA1*$^{[1]}$ or *Dh31*$^{-}$ larvae after 18h in a wet chamber
852 following or not (water) a 1h feeding period with yeast mixed with *Lp* or *Ecc* or *Bt.*
853 Shown is the average with 95% confidence interval of at least 3 independent
854 experiments with at least 20 larvae per trial and condition. The 0 symbol indicates an
855 absence of lethality. **** indicates p<0,0001, Fisher exact t-test. See the source data
856 file for details.

857 **E** and **F**: quantification over time of the amount of *Bt* (A) and *Ecc* (B) live bacteria
858 within the larval intestine of control or IMD pathway mutant animals including *ΔAMP14*
859 following a 1h feeding period with a solution containing yeast and bacteria. CFU stands
860 for Colony Forming Units. *ΔAMP14* is a mutant deleted for 14 antimicrobial-encoding
861 genes. Shown is the average ± SEM of at least 3 independent experiments with at
862 least 7 guts each. After 8h, either all the mutants were dead or the intestines were
863 severely damaged preventing the CFU counting. * Indicates p<0,05, Mann Whitney,
864 two-tailed test. See the source data file for details.

865

866

867

868

869 **FIGURE 8**

870 **Chronological coordination of ROS/TrpA1/Dh31 and IMD pathways for an**
871 **efficient microbial elimination.**

872 **t0:** larvae ingest bacteria from the food mixture (anterior on the left, only bacteria
873 similar to *Ecc* or *Bt* are illustrated). This initial phase necessitates a discrimination
874 between commensal and pathogenic bacteria, not elucidated in this study (symbolized
875 by '?'). The presence of pathogenic bacteria induces the production of ROS by
876 enterocytes (EC) in a Duox-dependent manner. Then ROS activates TrpA1 in
877 enteroendocrine cells (EEC). **t15 minutes:** Dh31 secretion by EEC is responsible for
878 the blockage of bacteria likely by promoting visceral muscle contractions leading to a
879 closure of a valve-like structure. This phenomenon concentrates the bacteria in the
880 anterior part of the gut. The bacterial concentration in this part of the intestinal lumen
881 may facilitate the triggering of the IMD signaling cascade that controls the transcription
882 of the genes (*AMPs*) encoding the antimicrobial peptides (AMPs). **t6 hours:** the valve-
883 like structure is still closed. The bactericidal activity of AMPs has eliminated most of
884 the bacteria accumulated in the anterior part of the intestine. Importantly, if
885 confinement is prevented, the larvae die; if the response by antimicrobial peptides is
886 hindered, the larvae die.

887

888

889 **SUPP1**

890 ***Ecc* and *Bt* are blocked in the anterior part of the intestine and disappear while**
891 ***Lp* transits to the posterior part and remains.**

892 **A**: Timelapse from the movies of L3 Larvae fed 1h with a mixture of yeast and *Ecc*
893 then transferred on a glass slide, in a wet chamber, to be imaged overnight. Refers
894 to Movie 1.

895 **B**: Timelapse from the movies of L3 Larvae fed 1h with a mixture of yeast and *Bt*
896 then transferred on a glass slide, in a wet chamber, to be imaged overnight. Refers
897 to Movie 2.

898 **C**: Timelapse from the movies of L3 Larvae fed 1h with a mixture of yeast and *Lp*
899 then transferred on a glass slide, in a wet chamber, to be imaged overnight. Refers
900 to Movie 3.

901 For A-C, the frames are separated by 5 minutes.

902

903 **SUPP2**

904 **Contrary to *Lp*, *Ecc* or *Bt* bacteria are blocked in the anterior part of the gut.**

905 **A**: Graphic representing the blockage ratio for dissected intestines of L3 larvae
906 exposed during 1h to a mixture composed of yeast and fluorescent bacteria. Shown is
907 the average blockage ratio with a 95% confidence interval from at least 3 independent
908 assays with at least 8 organs per condition and trial. **** indicates p<0,0001, Fisher
909 exact t-test. See the source data file for details.

910 **SUPP3**

911 ***Ecc* is not blocked anteriorly in *TrpA1*[1] and *Dh31*⁻ mutants, persists in the**
912 **posterior part of the intestine and disappears while *Lp* can be blocked following**
913 **exogenous addition of hCGRP.**

914 **A**: Timelapse from the movies of *TrpA1*[1] L3 Larvae fed 1h with a mixture of yeast
915 and *Ecc* then transferred on a glass slide, in a wet chamber, to be imaged overnight.
916 Refers to Movie 4.

917 **B**: Timelapse from the movies of *Dh31*⁻ L3 Larvae fed 1h with a mixture of yeast and
918 *Ecc* then transferred on a glass slide, in a wet chamber, to be imaged overnight.
919 Refers to Movie 5.

920 **C**: Timelapse from the movies of w⁻ L3 Larvae fed 1h with a mixture of yeast and *Lp* +
921 hCGRP then transferred on a glass slide, in a wet chamber, to be imaged overnight.
922 Refers to Movie 6.

923 For A-C, the frames are separated by 5 minutes.

924

925 **SUPP4**

926 **TARMsT2 are attached to the longitudinal gut muscles.**

927 Confocal fluorescent pictures of different TARMsT2 in the anterior portions of L3 larval
928 intestines to detect longitudinal and transversal muscles concentrated in actin. The
929 white star indicates the anterior part of the intestinal portion shown. The empty square

with dashed lines in A corresponds to the portion of the image magnified in A'. Scale bar represents 500µm.

**SUPP5**

***Bt* and *Ecc* are blocked anteriorly and persist in *PGRP-LC*$^{[\Delta E]}$ *and PGRP-LE*$^{[112]}$ mutants, respectively.**

**A**: Timelapse from the movies of *PGRP-LC*$^{[\Delta E]}$ L3 Larvae fed 1h with a mixture of yeast and *Bt* then transferred on a glass slide, in a wet chamber, to be imaged overnight. Refers to Movie 8.

**B**: Timelapse from the movies of *PGRP-LE*$^{[112]}$ L3 Larvae fed 1h with a mixture of yeast and *Ecc* then transferred on a glass slide, in a wet chamber, to be imaged overnight. Refers to Movie 9.

For A and B, the frames are separated by 5 minutes.

**SUPP6**

***Bt* and *Ecc* are blocked and persist anteriorly in *Dredd*$^{[F64]}$ *and Rel*$^{[E20]}$ mutants.**

**A**: Timelapse from the movies of *Dredd*$^{[F64]}$ L3 Larvae fed 1h with a mixture of yeast and *Ecc* then transferred on a glass slide, in a wet chamber, to be imaged overnight. Refers to Movie 10.

949 **B**: Timelapse from the movies of *Rel*$^{[E20]}$ L3 Larvae fed 1h with a mixture of yeast and
950 *Bt* then transferred on a glass slide, in a wet chamber, to be imaged overnight. Refers
951 to Movie 11.

952 **C**: Timelapse from the movies of *Rel*$^{[E20]}$ L3 Larvae fed 1h with a mixture of yeast and
953 *Ecc* then transferred on a glass slide, in a wet chamber, to be imaged overnight. Refers
954 to Movie 12.

955 For A-C, the frames are separated by 5 minutes.

956

957

958

959

960 **MOVIES**

961 **Movie 1**

962 https://doi.org/10.6084/m9.figshare.25018385.v2

963 **DOI: 10.6084/m9.figshare.25018385**

964 **Fluorescent *Ecc* is blocked in the anterior part of the larval intestine then**
965 **vanishes.**

966 Live imaging during 12h of a L3 control larva previously fed 1h with a food containing
967 *Ecc* fluorescent bacteria then transferred on a glass slide in a wet chamber.

968

969 **Movie 2**

970 https://doi.org/10.6084/m9.figshare.25018427.v2

971 **DOI: 10.6084/m9.figshare.25018427**

972 **Fluorescent *Bt* is blocked in the anterior part of the larval intestine then**
973 **vanishes.**

974 Live imaging during 12h of a L3 control larva previously fed 1h with a food containing
975 *Bt* fluorescent bacteria then transferred on a glass slide in a wet chamber.

976

977 **Movie 3**

978 https://doi.org/10.6084/m9.figshare.25018442.v2

979 **DOI: 10.6084/m9.figshare.25018442**

980 **Fluorescent *Lp* is not blocked in the anterior part of the larval intestine and**
981 **persists in the posterior midgut.**

982 Live imaging during 10h of a L3 control larva previously fed 1h with a food containing
983 *Lp* fluorescent bacteria then transferred on a glass slide in a wet chamber.

984

985 **Movie 4**

986 https://doi.org/10.6084/m9.figshare.25018463.v1

987 **DOI: 10.6084/m9.figshare.25018463**

988 **Fluorescent *Ecc* is not blocked in the anterior part of the *TrpA1* mutant larval**
989 **intestine and persists in the posterior midgut.**

990 Live imaging during 10h of a L3 *TrpA1* mutant larva previously fed 1h with a food
991 containing *Ecc* fluorescent bacteria then transferred on a glass slide in a wet chamber.

992

993 **Movie 5**

994 https://doi.org/10.6084/m9.figshare.25018472.v1

995 **DOI: 10.6084/m9.figshare.25018472**

996 **Fluorescent *Ecc* is not blocked in the anterior part of the *Dh31* mutant larval**
997 **intestine and persists in the posterior midgut.**

998 Live imaging during 10h of a L3 *Dh31* mutant larva previously fed 1h with a food
999 containing *Ecc* fluorescent bacteria then transferred on a glass slide in a wet chamber.

1000

1001 **Movie 6**

1002 https://doi.org/10.6084/m9.figshare.25018481.v1

1003 **DOI: 10.6084/m9.figshare.25018481**

1004 **Fluorescent *Lp* is blocked in the anterior part of the larval intestine following**
1005 **treatment with hCGRP.**

1006 Live imaging during 12h of a control L3 larva previously fed 1h with a food containing
1007 *Lp* fluorescent bacteria and hCGRP then transferred on a glass slide in a wet chamber.

1008

1009 **Movie 7**

1010 https://doi.org/10.6084/m9.figshare.25018496.v1

1011 **DOI: 10.6084/m9.figshare.25018496**

1012 **TARMsT2 are attached to the longitudinal gut muscles.**

1013 Confocal imaging of the intestine from a control animal stained with fluorescent
1014 phalloidin and animated 3D-reconstruction of the anterior portion containing the
1015 attached TARMs.

1016

1017 **Movie 8**

1018 https://doi.org/10.6084/m9.figshare.25018499.v1

1019 **DOI: 10.6084/m9.figshare.25018499**

1020 **Fluorescent *Bt* is blocked in the anterior part of the *PGRP-LC* mutant larval**
1021 **intestine and persists.**

1022 Live imaging during 12h of a L3 *PGRP-LC* mutant larva previously fed 1h with a food
1023 containing *Bt* fluorescent bacteria then transferred on a glass slide in a wet chamber.

1024

1025 **Movie 9**

1026 https://doi.org/10.6084/m9.figshare.25018505.v1

1027 **DOI: 10.6084/m9.figshare.25018505**

1028 **Fluorescent *Ecc* is blocked in the anterior part of the *PGRP-LE* mutant larval**
1029 **intestine and persists.**

1030 Live imaging during 12h of a L3 *PGRP-LE* mutant larva previously fed 1h with a food
1031 containing *Ecc* fluorescent bacteria then transferred on a glass slide in a wet chamber.

1032

1033 **Movie 10**

1034 https://doi.org/10.6084/m9.figshare.25018517.v1

1035 **DOI: 10.6084/m9.figshare.25018517**

1036 **Fluorescent *Ecc* is blocked in the anterior part of the *Dredd* mutant larval**
1037 **intestine and persists.**

1038 Live imaging during 12h of a L3 *Dredd* mutant larva previously fed 1h with a food
1039 containing *Ecc* fluorescent bacteria then transferred on a glass slide in a wet chamber.

1040

1041 **Movie 11**

1042 https://doi.org/10.6084/m9.figshare.25018529.v1

1043 **DOI: 10.6084/m9.figshare.25018529**

1044 **Fluorescent *Bt* is blocked in the anterior part of the *Rel* mutant larval intestine**
1045 **and persists.**

1046 Live imaging during 12h of a L3 *Rel* mutant larva previously fed 1h with a food
1047 containing *Bt* fluorescent bacteria then transferred on a glass slide in a wet chamber.

1048

1049 **Movie 12**

1050 https://doi.org/10.6084/m9.figshare.25018538.v1

1051 **DOI: 10.6084/m9.figshare.25018538**

1052 **Fluorescent *Ecc* is blocked in the anterior part of the *Rel* mutant larval intestine**
1053 **and persists.**

1054 Live imaging during 12h of a L3 *Rel* mutant larva previously fed 1h with a food
1055 containing *Ecc* fluorescent bacteria then transferred on a glass slide in a wet chamber.

## AUTHOR CONTRIBUTIONS

L.K., A.G., F.T., M.M., O.P., D.O. and J.R. conceived the experiments. F.T., M.M., O.P. performed the experiments. L.K., A.G., F.T., D.O. and J.R. wrote the manuscript. A.G., D.O. and J.R. secured funding.

## COMPETING INTERESTS

The authors have declared that no competing interests exist.


## ACKNOWLEDGMENTS

We are grateful to all members of the BES and DEB teams at the Institut Sophia Agrobiotech for fruitful discussions. We greatly thank Emilie Avazéri, Gladys Gazelle, Marie-Paule Esposito, Juliette Dubois and Elisa Di Lelio for their technical support. We thank Bernard Charroux (at the IBDM Aix Marseille University) and Ambra MASUZZO (in the team of Richard Benton, Université de Lausanne) for pioneer observations and numerous discussions, François Leulier and Renata Matos for sharing bacterial and fly lines and Frank Schnorrer for discussions about alary muscles.

## FUNDING

F.T. was supported by the Lebanese Association for Scientific Research (LASER), the AJAJE association from Lebanon, and the Université Côte d'Azur (ATER). This work was supported by the French government through the UCAJEDI Investments in the Future project managed by the National Research Agency (ANR) with the reference number ANR-15-IDEX-01 and through the ANR-22-CE35-0006-01 (BaDAss) to A.G. This work was supported by CNRS, ANR BACNEURODRO (ANR-17-CE16-0023-01), Equipe Fondation pour la Recherche Médicale (EQU201603007783) and the ANR Pepneuron (ANR-21-CE16-0027) to J.R. and L.K.

## REFERENCES

**Arias-Rojas, A., Frahm, D., Hurwitz, R., Brinkmann, V. and Iatsenko, I.** (2023). Resistance to host antimicrobial peptides mediates resilience of gut commensals during infection and aging in Drosophila. *Proc Natl Acad Sci U S A* **120**, e2305649120.

**Basset, A., Khush, R. S., Braun, A., Gardan, L., Boccard, F., Hoffmann, J. A. and Lemaitre, B.** (2000). The phytopathogenic bacteria Erwinia carotovora infects Drosophila and activates an immune response. *Proc Natl Acad Sci U S A* **97**, 3376-81.

**Bataillé, L., Colombié, N., Pelletier, A., Paululat, A., Lebreton, G., Carrier, Y., Frendo, J. L. and Vincent, A.** (2020). Alary muscles and thoracic alary-related muscles are atypical striated muscles involved in maintaining the position of internal organs. *Development* **147**.

**Belinskaia, M., Wang, J., Kaza, S. K., Antoniazzi, C., Zurawski, T., Dolly, J. O. and Lawrence, G. W.** (2023). Bipartite Activation of Sensory Neurons by a TRPA1 Agonist Allyl Isothiocyanate Is Reflected by Complex Ca(2+) Influx and CGRP Release Patterns: Enhancement by NGF and Inhibition with VAMP and SNAP-25 Cleaving Botulinum Neurotoxins. *Int J Mol Sci* **24**.

**Benguettat, O., Jneid, R., Soltys, J., Loudhaief, R., Brun-Barale, A., Osman, D. and Gallet, A.** (2018). The DH31/CGRP enteroendocrine peptide triggers intestinal contractions favoring the elimination of opportunistic bacteria. *PLoS Pathog.* **14**, e1007279. doi: 10.1371/journal.ppat.1007279. eCollection 2018 Sep.

**Bosco-Drayon, V., Poidevin, M., Boneca, I. G., Narbonne-Reveau, K., Royet, J. and Charroux, B.** (2012). Peptidoglycan sensing by the receptor PGRP-LE in the Drosophila gut induces immune responses to infectious bacteria and tolerance to microbiota. *Cell Host Microbe* **12**, 153-65.

**Bulc, M., Palus, K., Całka, J. and Zielonka, Ł.** (2018). Changes in Immunoreactivity of Sensory Substances within the Enteric Nervous System of the Porcine Stomach during Experimentally Induced Diabetes. *J Diabetes Res* **2018**, 4735659.

**Capo, F., Wilson, A. and Di Cara, F.** (2019). The Intestine of Drosophila melanogaster: An Emerging Versatile Model System to Study Intestinal Epithelial Homeostasis and Host-Microbial Interactions in Humans. *Microorganisms.* **7(9).** microorganisms7090336. doi: 10.3390/microorganisms7090336.

1114 **Carboni, A. L., Hanson, M. A., Lindsay, S. A., Wasserman, S. A. and Lemaitre, B.**
1115 (2022). Cecropins contribute to Drosophila host defense against a subset of fungal and
1116 Gram-negative bacterial infection. *Genetics* **220**.
1117 **Chakrabarti, S., Liehl, P., Buchon, N. and Lemaitre, B.** (2012). Infection-induced host
1118 translational blockage inhibits immune responses and epithelial renewal in the Drosophila
1119 gut. *Cell Host Microbe* **12**, 60-70. doi: 10.1016/j.chom.2012.06.001.
1120 **Chen, J., Kim, S. M. and Kwon, J. Y.** (2016). A Systematic Analysis of Drosophila
1121 Regulatory Peptide Expression in Enteroendocrine Cells. 10.14348/molcells.2016.0014.
1122 **Dombrovski, M., Kim, A., Poussard, L., Vaccari, A., Acton, S., Spillman, E., Condron,**
1123 **B. and Yuan, Q.** (2019). A Plastic Visual Pathway Regulates Cooperative Behavior in
1124 Drosophila Larvae. *Curr Biol* **29**, 1866-1876.e5.
1125 **Dombrovski, M., Poussard, L., Moalem, K., Kmecova, L., Hogan, N., Schott, E.,**
1126 **Vaccari, A., Acton, S. and Condron, B.** (2017). Cooperative Behavior Emerges among
1127 Drosophila Larvae. *Curr Biol* **27**, 2821-2826.e2.
1128 **Du, E. J., Ahn, T. J., Kwon, I., Lee, J. H., Park, J. H., Park, S. H., Kang, T. M., Cho, H.,**
1129 **Kim, T. J., Kim, H. W. et al.** (2016a). TrpA1 Regulates Defecation of Food-Borne
1130 Pathogens under the Control of the Duox Pathway. *PLoS Genet* **12**, e1005773. doi:
1131 10.1371/journal.pgen.1005773. eCollection 2016 Jan.
1132 **Du, E. J., Ahn, T. J., Wen, X., Seo, D. W., Na, D. L., Kwon, J. Y., Choi, M., Kim, H. W.,**
1133 **Cho, H. and Kang, K.** (2016b). Nucleophile sensitivity of Drosophila TRPA1 underlies light-
1134 induced feeding deterrence. *Elife* **5**.
1135 **Earl, S. C., Rogers, M. T., Keen, J., Bland, D. M., Houppert, A. S., Miller, C., Temple, I.,**
1136 **Anderson, D. M. and Marketon, M. M.** (2015). Resistance to Innate Immunity Contributes
1137 to Colonization of the Insect Gut by Yersinia pestis. *PLoS One* **10**, e0133318.
1138 **Gu, P., Gong, J., Shang, Y., Wang, F., Ruppell, K. T., Ma, Z., Sheehan, A. E., Freeman,**
1139 **M. R. and Xiang, Y.** (2019). Polymodal Nociception in Drosophila Requires Alternative
1140 Splicing of TrpA1. *Curr Biol* **29**, 3961-3973.e6.
1141 **Guntur, A. R., Gu, P., Takle, K., Chen, J., Xiang, Y. and Yang, C. H.** (2015). Drosophila
1142 TRPA1 isoforms detect UV light via photochemical production of H2O2. *Proc Natl Acad Sci*
1143 *U S A* **112**, E5753-61.
1144 **Guo, X., Lv, J. and Xi, R.** (2021). The specification and function of enteroendocrine cells in
1145 Drosophila and mammals: a comparative review. *Febs j*.
1146 **Ha, E. M., Lee, K. A., Seo, Y. Y., Kim, S. H., Lim, J. H., Oh, B. H., Kim, J. and Lee, W. J.**
1147 (2009). Coordination of multiple dual oxidase-regulatory pathways in responses to
1148 commensal and infectious microbes in drosophila gut. *Nat Immunol* **10**, 949-57. doi:
1149 10.1038/ni.1765. Epub 2009 Aug 9.
1150 **Ha, E. M., Oh, C. T., Bae, Y. S. and Lee, W. J.** (2005). A direct role for dual oxidase in
1151 Drosophila gut immunity. *Science* **310**, 847-50.
1152 **Hachfi, S., Brun-Barale, A., Munro, P., Nawrot-Esposito, M.-P., Michel, G., Fichant, A.,**
1153 **Bonis, M., Ruimy, R., Boyer, L. and Gallet, A.** (2023). Ingestion of Bacillus cereus spores
1154 dampens the immune response to favor bacterial persistence. *BioRxiv (Nature comm., In*
1155 *revision)*.
1156 **Hanson, M. A. and Lemaitre, B.** (2020). New insights on Drosophila antimicrobial peptide
1157 function in host defense and beyond. *Curr Opin Immunol* **62**, 22-30.
1158 **Hegedus, D., Erlandson, M., Gillott, C. and Toprak, U.** (2009). New insights into
1159 peritrophic matrix synthesis, architecture, and function. *Annu Rev Entomol* **54**, 285-302.
1160 **Kaneko, T., Yano, T., Aggarwal, K., Lim, J. H., Ueda, K., Oshima, Y., Peach, C., Erturk-**
1161 **Hasdemir, D., Goldman, W. E., Oh, B. H. et al.** (2006). PGRP-LC and PGRP-LE have
1162 essential yet distinct functions in the drosophila immune response to monomeric DAP-type
1163 peptidoglycan. *Nat Immunol* **7**, 715-23.
1164 **Kasacka, I.** (2009). Quantitative distribution and localization of calcitonin gene-related
1165 peptide-like cells in the stomach of two kidney, one clip rats. *J Physiol Pharmacol* **60**, 35-9.
1166 **Keita, S., Masuzzo, A., Royet, J. and Kurz, C. L.** (2017). Drosophila larvae food intake
1167 cessation following exposure to Erwinia contaminated media requires odor perception, Trpa1

1168 channel and evf virulence factor. *J Insect Physiol.* **99:25-32.**,
1169 10.1016/j.jinsphys.2017.02.004. Epub 2017 Feb 21.
1170 **Kondo, T., Oshima, T., Obata, K., Sakurai, J., Knowles, C. H., Matsumoto, T., Noguchi,**
1171 **K. and Miwa, H.** (2010). Role of transient receptor potential A1 in gastric nociception.
1172 *Digestion* **82**, 150-5.
1173 **Kunst, M., Hughes, M. E., Raccuglia, D., Felix, M., Li, M., Barnett, G., Duah, J. and**
1174 **Nitabach, M. N.** (2014). Calcitonin gene-related peptide neurons mediate sleep-specific
1175 circadian output in Drosophila. *Curr Biol* **24**, 2652-64.
1176 **LaJeunesse, D. R., Johnson, B., Presnell, J. S., Catignas, K. K. and Zapotoczny, G.**
1177 (2010). Peristalsis in the junction region of the Drosophila larval midgut is modulated by
1178 DH31 expressing enteroendocrine cells. *BMC Physiol* **10:14.**, 10.1186/1472-6793-10-14.
1179 **Lapointe, T. K. and Altier, C.** (2011). The role of TRPA1 in visceral inflammation and pain.
1180 *Channels* **5**, 525-9. doi: 10.4161/chan.5.6.18016. Epub 2011 Nov 1.
1181 **Lee, K. A., Kim, S. H., Kim, E. K., Ha, E. M., You, H., Kim, B., Kim, M. J., Kwon, Y., Ryu,**
1182 **J. H. and Lee, W. J.** (2013). Bacterial-derived uracil as a modulator of mucosal immunity
1183 and gut-microbe homeostasis in Drosophila. *Cell* **153**, 797-811. doi:
1184 10.1016/j.cell.2013.04.009.
1185 **Lemaitre, B. and Miguel-Aliaga, I.** (2013). The digestive tract of Drosophila melanogaster.
1186 *Annu Rev Genet* **47:377-404.**, 10.1146/annurev-genet-111212-133343.
1187 **Leulier, F., Parquet, C., Pili-Floury, S., Ryu, J. H., Caroff, M., Lee, W. J., Mengin-**
1188 **Lecreulx, D. and Lemaitre, B.** (2003). The Drosophila immune system detects bacteria
1189 through specific peptidoglycan recognition. *Nat Immunol* **4**, 478-84.
1190 **Louis, M. and de Polavieja, G.** (2017). Collective Behavior: Social Digging in Drosophila
1191 Larvae. *Curr Biol* **27**, R1010-r1012.
1192 **Mast, J. D., De Moraes, C. M., Alborn, H. T., Lavis, L. D. and Stern, D. L.** (2014). Evolved
1193 differences in larval social behavior mediated by novel pheromones. *Elife* **3**, e04205.
1194 **Nässel, D. R. and Zandawala, M.** (2019). Recent advances in neuropeptide signaling in
1195 Drosophila, from genes to physiology and behavior. *Prog Neurobiol* **179**, 101607.
1196 **Nawrot-Esposito, M. P., Babin, A., Pasco, M., Poirié, M., Gatti, J. L. and Gallet, A.**
1197 (2020). Bacillus thuringiensis Bioinsecticides Induce Developmental Defects in Non-Target
1198 Drosophila melanogaster Larvae. *Insects* **11**.
1199 **Neyen, C., Bretscher, A. J., Binggeli, O. and Lemaitre, B.** (2014). Methods to study
1200 Drosophila immunity. *Methods* **68**, 116-28. doi: 10.1016/j.ymeth.2014.02.023. Epub 2014
1201 Mar 12.
1202 **Ogawa, N., Kurokawa, T. and Mori, Y.** (2016). Sensing of redox status by TRP channels.
1203 *Cell Calcium* **60**, 115-22. doi: 10.1016/j.ceca.2016.02.009. Epub 2016 Mar 4.
1204 **Park, D., Veenstra, J. A., Park, J. H. and Taghert, P. H.** (2008). Mapping peptidergic cells
1205 in Drosophila: where DIMM fits in. *PLoS One.* **3**, e1896. doi: 10.1371/journal.pone.0001896.
1206 **Pelaseyed, T., Bergstrom, J. H., Gustafsson, J. K., Ermund, A., Birchenough, G. M.,**
1207 **Schutte, A., van der Post, S., Svensson, F., Rodriguez-Pineiro, A. M., Nystrom, E. E. et**
1208 **al.** (2014). The mucus and mucins of the goblet cells and enterocytes provide the first
1209 defense line of the gastrointestinal tract and interact with the immune system. *Immunol Rev*
1210 **260**, 8-20. doi: 10.1111/imr.12182.
1211 **Ramond, E., Jamet, A., Ding, X., Euphrasie, D., Bouvier, C., Lallemant, L., He, X.,**
1212 **Arbibe, L., Coureuil, M. and Charbit, A.** (2021). Reactive Oxygen Species-Dependent
1213 Innate Immune Mechanisms Control Methicillin-Resistant Staphylococcus aureus Virulence
1214 in the Drosophila Larval Model. *MBio* **12**, e0027621.
1215 **Ryu, J. H., Ha, E. M., Oh, C. T., Seol, J. H., Brey, P. T., Jin, I., Lee, D. G., Kim, J., Lee, D.**
1216 **and Lee, W. J.** (2006). An essential complementary role of NF-kappaB pathway to
1217 microbicidal oxidants in Drosophila gut immunity. *EMBO J* **25**, 3693-701. Epub 2006 Jul 20.
1218 **Stenbak, C. R., Ryu, J. H., Leulier, F., Pili-Floury, S., Parquet, C., Hervé, M., Chaput, C.,**
1219 **Boneca, I. G., Lee, W. J., Lemaitre, B. et al.** (2004). Peptidoglycan molecular requirements
1220 allowing detection by the Drosophila immune deficiency pathway. *J Immunol* **173**, 7339-48.
1221 **Storelli, G., Strigini, M., Grenier, T., Bozonnet, L., Schwarzer, M., Daniel, C., Matos, R.**
1222 **and Leulier, F.** (2018). Drosophila Perpetuates Nutritional Mutualism by Promoting the

1223 Fitness of Its Intestinal Symbiont Lactobacillus plantarum. *Cell Metab.* **27**, 362-377.e8. doi:
1224 10.1016/j.cmet.2017.11.011. Epub 2017 Dec 28.
1225 **Surendran, S., Huckesfeld, S., Waschle, B. and Pankratz, M. J.** (2017). Pathogen-
1226 induced food evasion behavior in Drosophila larvae. *J Exp Biol.* **220**, 1774-1780. doi:
1227 10.1242/jeb.153395. Epub 2017 Mar 2.
1228 **Veenstra, J. A., Agricola, H. J. and Sellami, A.** (2008). Regulatory peptides in fruit fly
1229 midgut. *Cell Tissue Res* **334**, 499-516. doi: 10.1007/s00441-008-0708-3. Epub 2008 Oct 30.
1230 **Vodovar, N., Vinals, M., Liehl, P., Basset, A., Degrouard, J., Spellman, P., Boccard, F.**
1231 **and Lemaitre, B.** (2005). Drosophila host defense after oral infection by an
1232 entomopathogenic Pseudomonas species. *Proc Natl Acad Sci U S A* **102**, 11414-9. Epub
1233 2005 Aug 1.
1234 **Younes, S., Al-Sulaiti, A., Nasser, E. A. A., Najjar, H. and Kamareddine, L.** (2020).
1235 Drosophila as a Model Organism in Host-Pathogen Interaction Studies. *Front Cell Infect*
1236 *Microbiol* **10**, 214.
1237 **Zhai, Z., Huang, X. and Yin, Y.** (2018). Beyond immunity: The Imd pathway as a
1238 coordinator of host defense, organismal physiology and behavior. *Dev Comp Immunol* **83**,
1239 51-59.
1240

# FIGURE 1

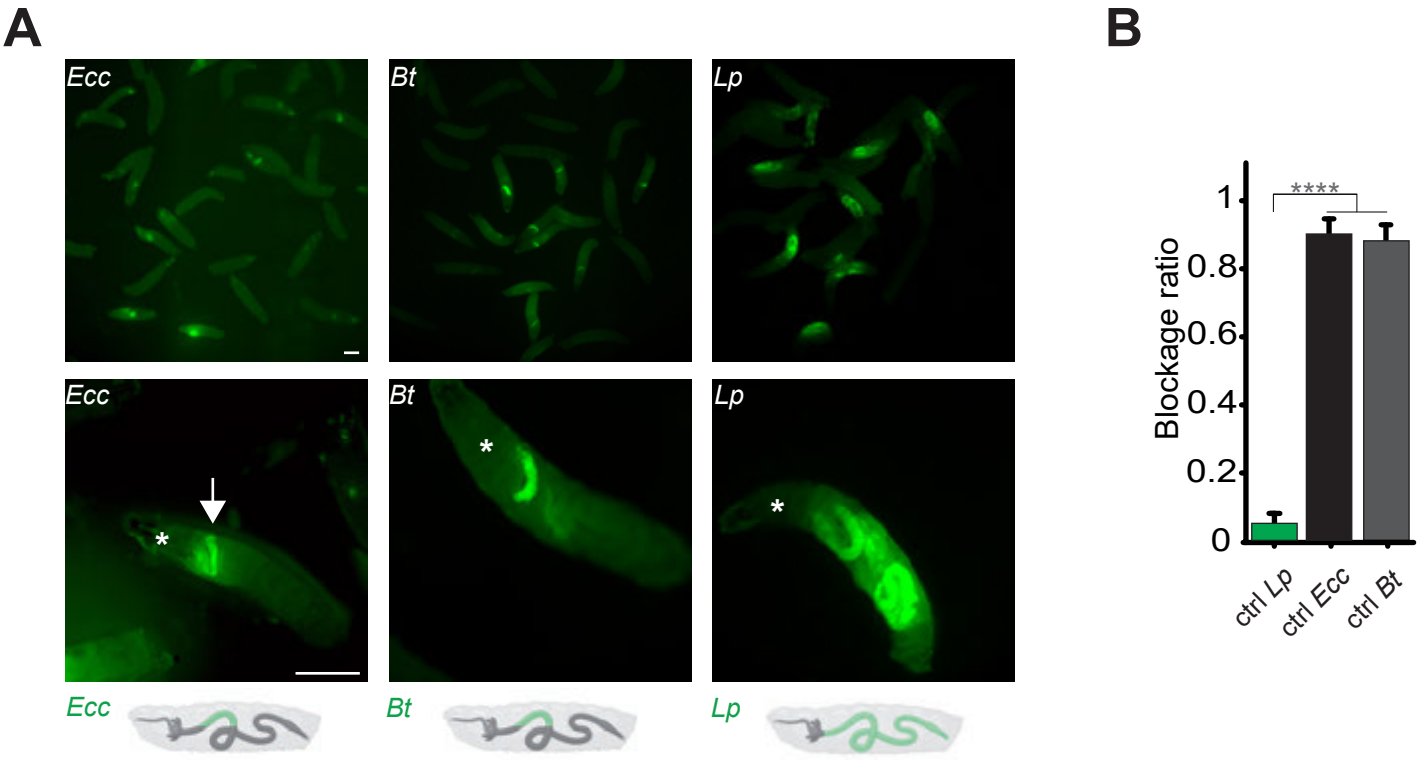
A
Ecc
Bt
Lp
Ecc
Bt
Lp
Ecc
Bt
Lp
B
****
Blockage ratio
1
0.8
0.6
0.4
0.2
0
ctrl Lp
ctrl Ecc
ctrl Bt

# FIGURE 2

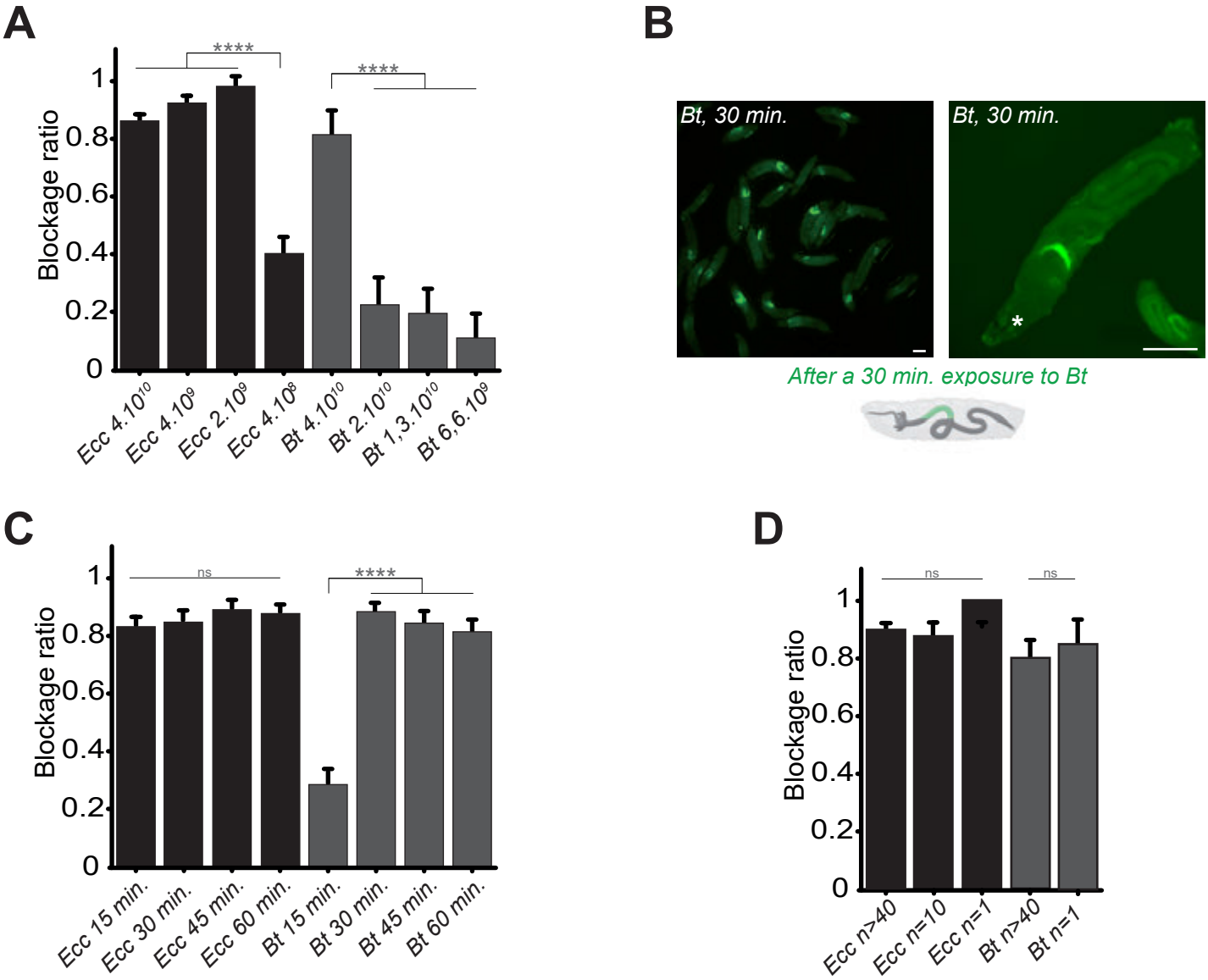
A
****
****
Blockage ratio
1
0.8
0.6
0.4
0.2
0
Ecc 4.10^10
Ecc 4.10^9
Ecc 2.10^9
Ecc 4.10^8
Bt 4.10^10
Bt 2.10^10
Bt 1,3.10^10
Bt 6,6.10^9
B
Bt, 30 min.
Bt, 30 min.
*
After a 30 min. exposure to Bt
C
ns
****
Blockage ratio
1
0.8
0.6
0.4
0.2
0
Ecc 15 min.
Ecc 30 min.
Ecc 45 min.
Ecc 60 min.
Bt 15 min.
Bt 30 min.
Bt 45 min.
Bt 60 min.
D
ns
ns
Blockage ratio
1
0.8
0.6
0.4
0.2
0
Ecc n>40
Ecc n=10
Ecc n=1
Bt n>40
Bt n=1

# FIGURE 3

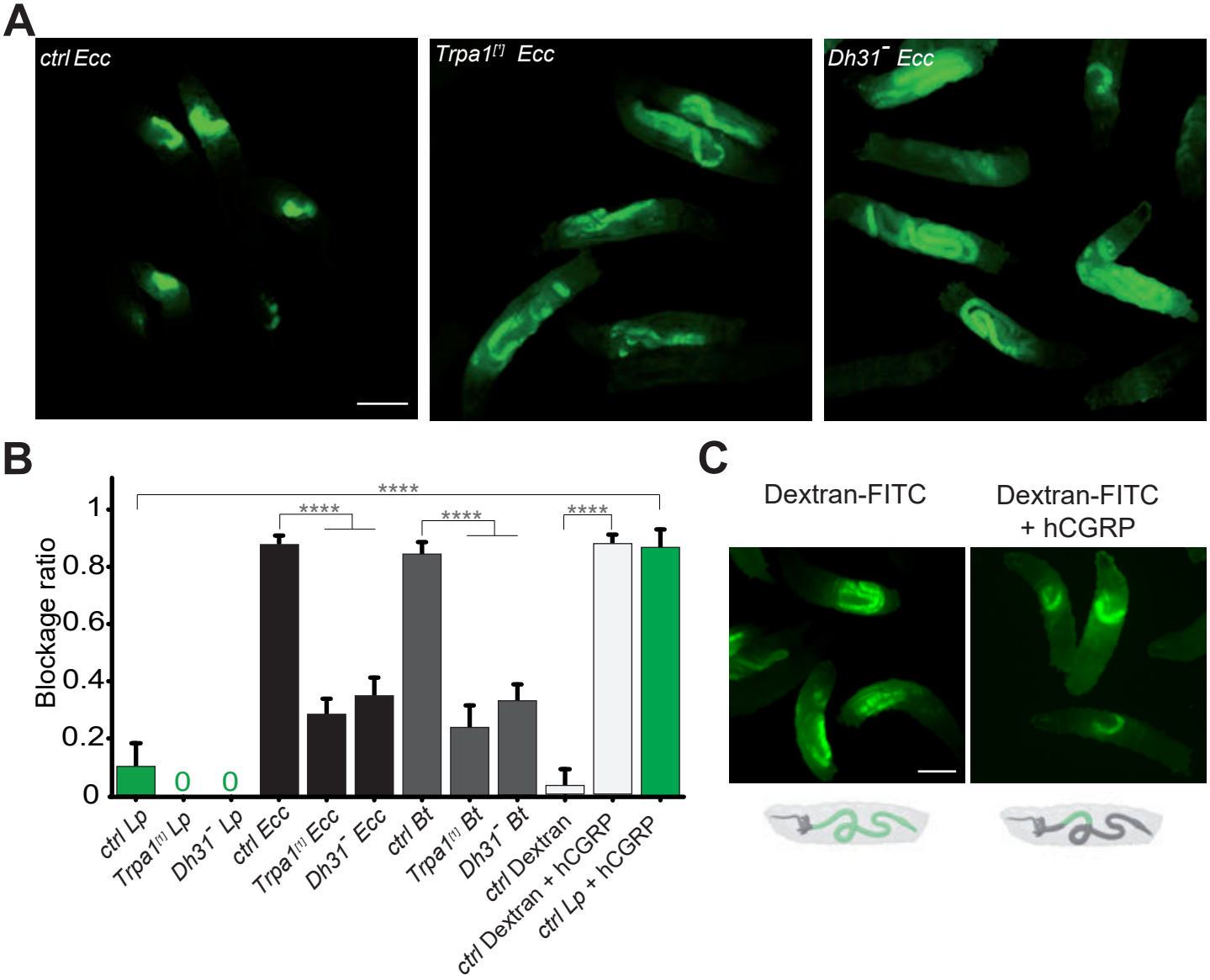
A
ctrl Ecc
Trpa1[1] Ecc
Dh31¯ Ecc
B
Blockage ratio
1
0.8
0.6
0.4
0.2
0
****
****
****
****
0
0
ctrl Lp
Trpa1[1] Lp
Dh31¯ Lp
ctrl Ecc
Trpa1[1] Ecc
Dh31¯ Ecc
ctrl Bt
Trpa1[1] Bt
Dh31¯ Bt
ctrl Dextran
ctrl Dextran + hCGRP
ctrl Lp + hCGRP
C
Dextran-FITC
Dextran-FITC
+ hCGRP

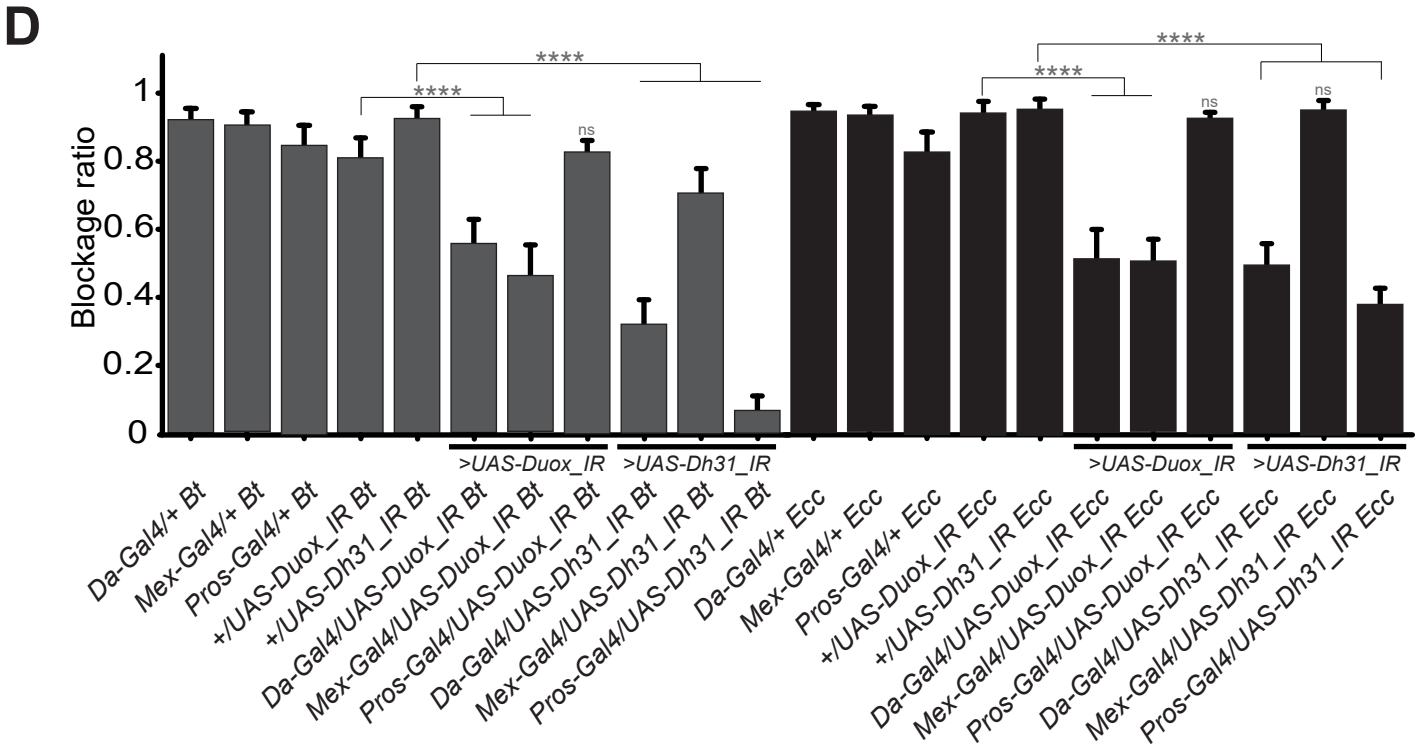
D
Blockage ratio
1
0.8
0.6
0.4
0.2
0
****
****
ns
****
****
ns
ns
>UAS-Duox_IR
>UAS-Dh31_IR
>UAS-Duox_IR
>UAS-Dh31_IR
Da-Gal4/+ Bt
Mex-Gal4/+ Bt
Pros-Gal4/+ Bt
+/UAS-Duox_IR Bt
+/UAS-Dh31_IR Bt
Da-Gal4/UAS-Duox_IR Bt
Mex-Gal4/UAS-Duox_IR Bt
Pros-Gal4/UAS-Duox_IR Bt
Da-Gal4/UAS-Dh31_IR Bt
Mex-Gal4/UAS-Dh31_IR Bt
Pros-Gal4/UAS-Dh31_IR Bt
Da-Gal4/+ Ecc
Mex-Gal4/+ Ecc
Pros-Gal4/+ Ecc
+/UAS-Duox_IR Ecc
+/UAS-Dh31_IR Ecc
Da-Gal4/UAS-Duox_IR Ecc
Mex-Gal4/UAS-Duox_IR Ecc
Pros-Gal4/UAS-Duox_IR Ecc
Da-Gal4/UAS-Dh31_IR Ecc
Mex-Gal4/UAS-Dh31_IR Ecc
Pros-Gal4/UAS-Dh31_IR Ecc

# FIGURE 4

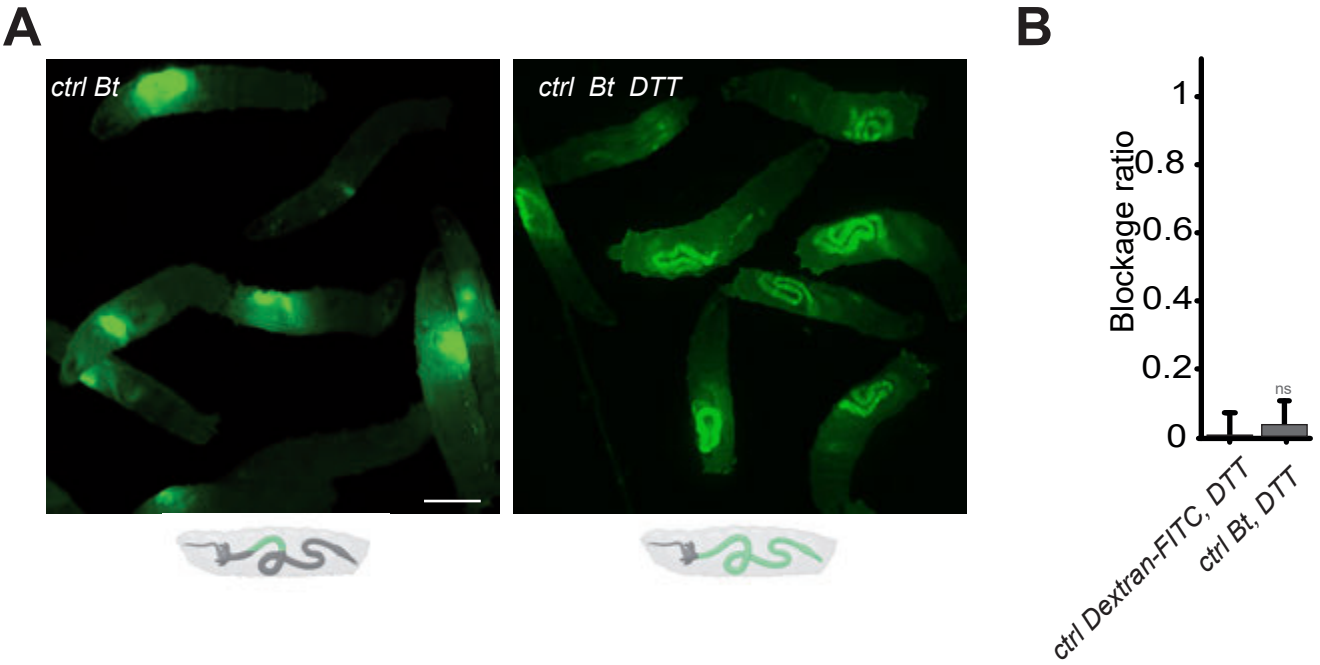
A
ctrl Bt
ctrl Bt DTT
B
Blockage ratio
1
0.8
0.6
0.4
0.2
0
ns
ctrl Dextran-FITC, DTT
ctrl Bt, DTT

# FIGURE 5

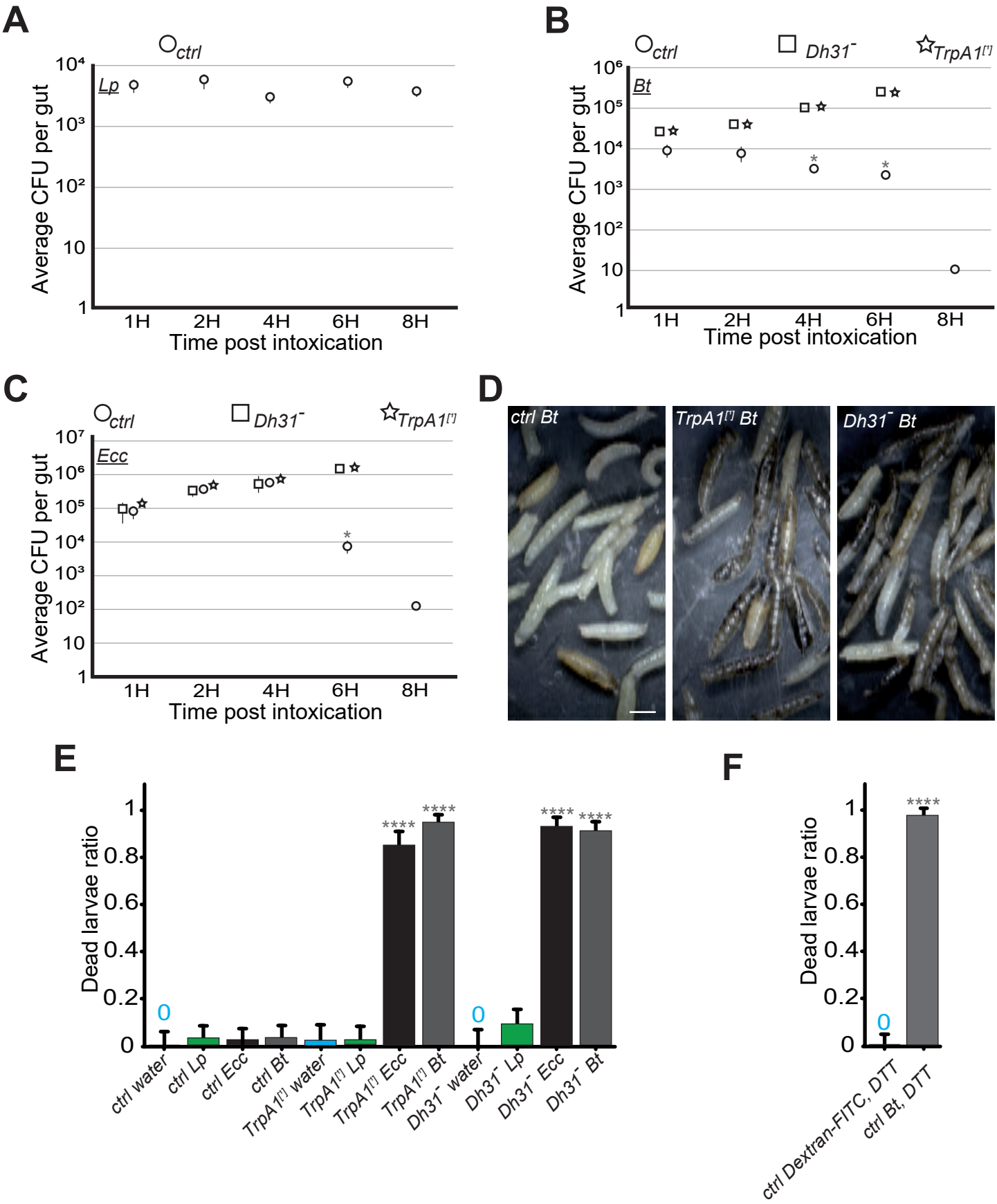
A
ctrl
Lp
Average CFU per gut
Time post intoxication
1H
2H
4H
6H
8H
B
ctrl
Dh31⁻
TrpA1[ts]
Bt
C
Ecc
D
ctrl Bt
TrpA1[ts] Bt
Dh31⁻ Bt
E
Dead larvae ratio
ctrl water
ctrl Lp
ctrl Ecc
ctrl Bt
TrpA1[ts] water
TrpA1[ts] Lp
TrpA1[ts] Ecc
TrpA1[ts] Bt
Dh31⁻ water
Dh31⁻ Lp
Dh31⁻ Ecc
Dh31⁻ Bt
F
ctrl Dextran-FITC, DTT
ctrl Bt, DTT

# FIGURE 6

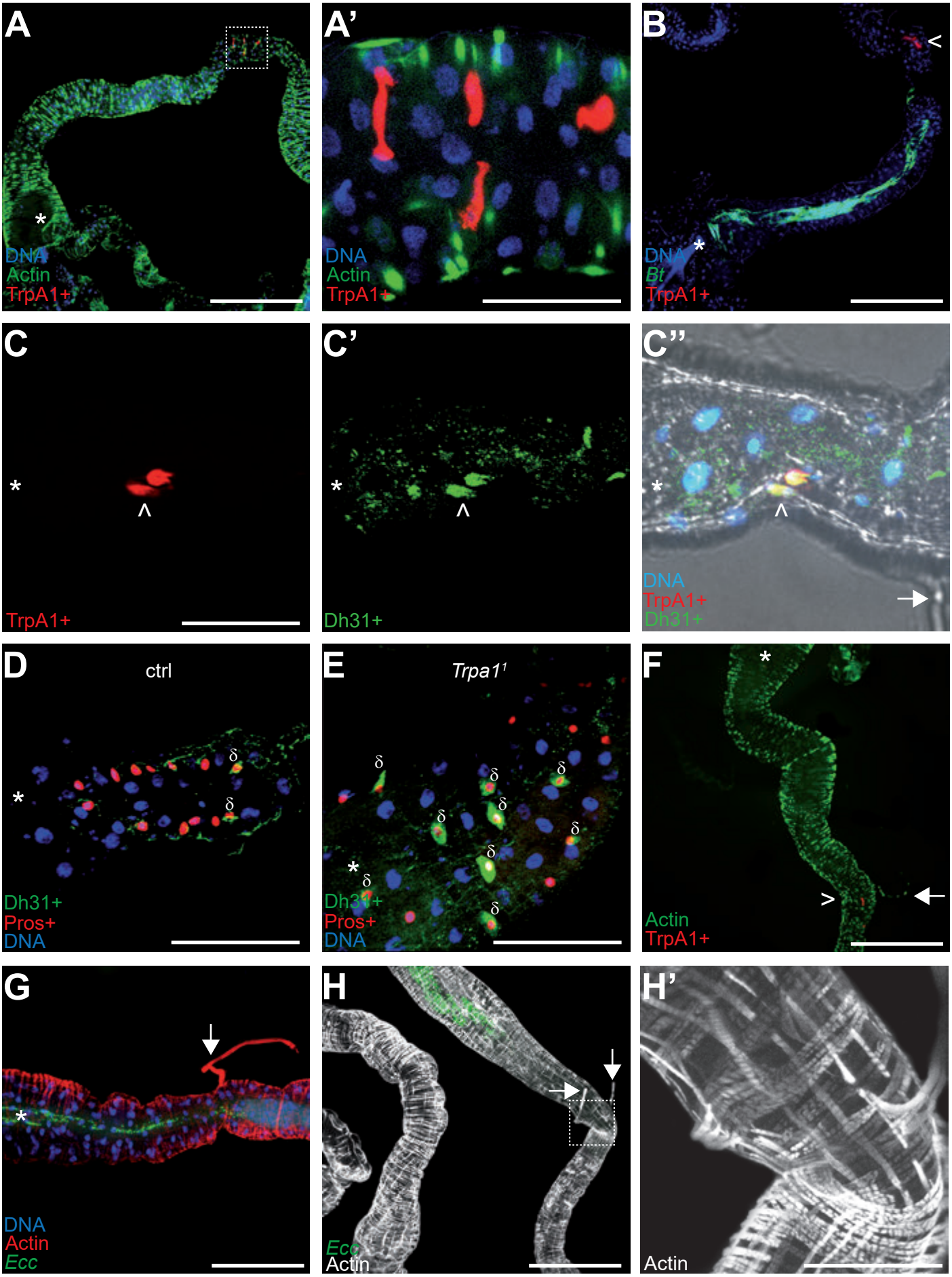
A
DNA
Actin
TrpA1+
A'
DNA
Actin
TrpA1+
B
DNA
Bt
TrpA1+
C
TrpA1+
C'
Dh31+
C''
DNA
TrpA1+
Dh31+
D
ctrl
Dh31+
Pros+
DNA
E
Trpa1¹
Dh31+
Pros+
DNA
F
Actin
TrpA1+
G
DNA
Actin
Ecc
H
Ecc
Actin
H'
Actin

# FIGURE 7

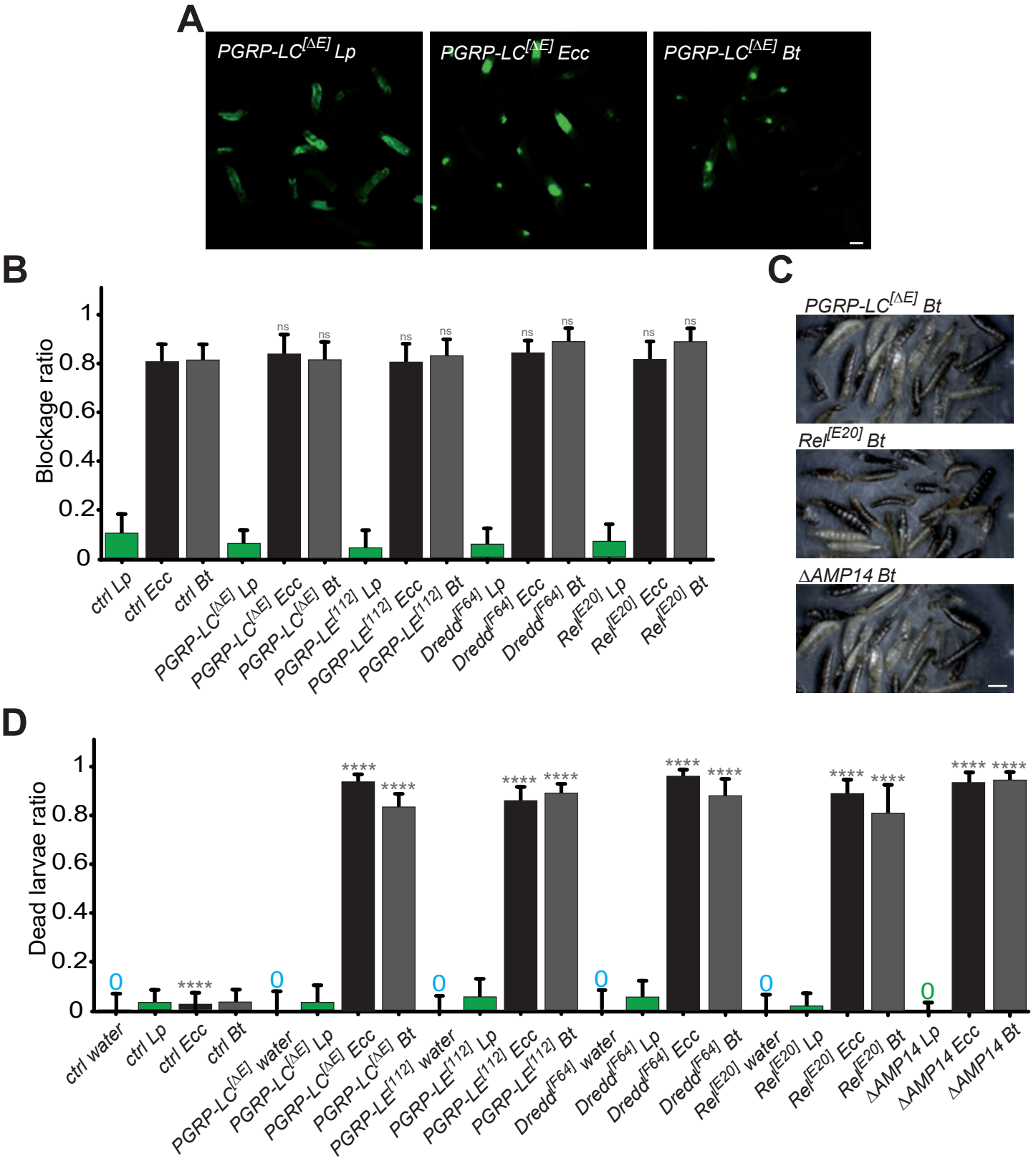
A
PGRP-LC[ΔE] Lp
PGRP-LC[ΔE] Ecc
PGRP-LC[ΔE] Bt
B
Blockage ratio
ctrl Lp
ctrl Ecc
ctrl Bt
PGRP-LC[ΔE] Lp
PGRP-LC[ΔE] Ecc
PGRP-LC[ΔE] Bt
PGRP-LE[112] Lp
PGRP-LE[112] Ecc
PGRP-LE[112] Bt
Dredd[F64] Lp
Dredd[F64] Ecc
Dredd[F64] Bt
Rel[E20] Lp
Rel[E20] Ecc
Rel[E20] Bt
ns
C
PGRP-LC[ΔE] Bt
Rel[E20] Bt
ΔAMP14 Bt
D
Dead larvae ratio
ctrl water
ctrl Lp
ctrl Ecc
ctrl Bt
PGRP-LC[ΔE] water
PGRP-LC[ΔE] Lp
PGRP-LC[ΔE] Ecc
PGRP-LC[ΔE] Bt
PGRP-LE[112] water
PGRP-LE[112] Lp
PGRP-LE[112] Ecc
PGRP-LE[112] Bt
Dredd[F64] water
Dredd[F64] Lp
Dredd[F64] Ecc
Dredd[F64] Bt
Rel[E20] water
Rel[E20] Lp
Rel[E20] Ecc
Rel[E20] Bt
ΔAMP14 Lp
ΔAMP14 Ecc
ΔAMP14 Bt
****
E
ctrl
LC[ΔE]
LE[112]
Rel[E20]
ΔAMP14
B.t.
Average CFU per gut
Time post intoxication
1H
2H
4H
6H
8H
F
Ecc15

# FIGURE 8

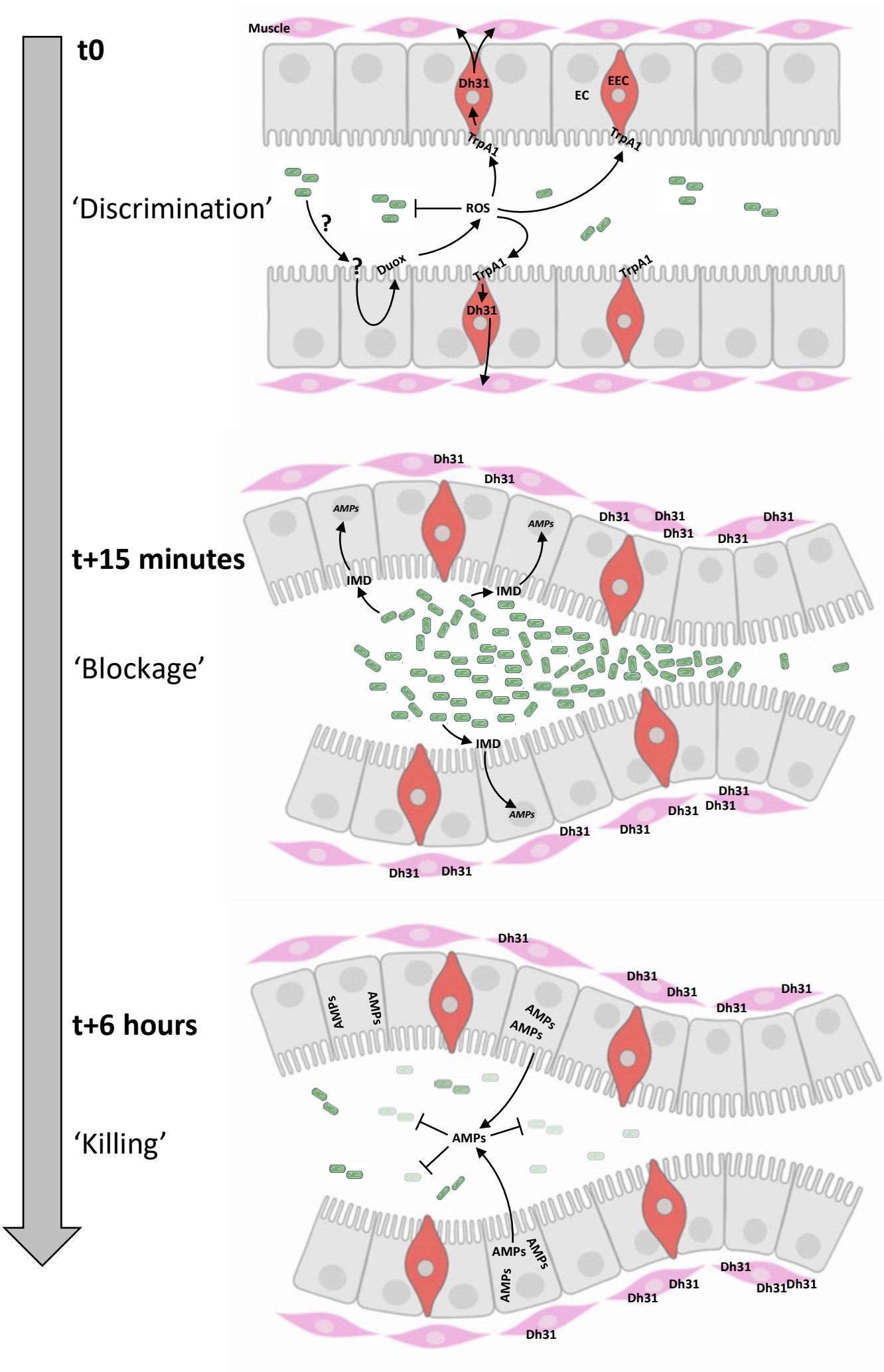
t0
'Discrimination'
Muscle
Dh31
EEC
EC
TrpA1
TrpA1
ROS
?
?
Duox
TrpA1
TrpA1
Dh31
t+15 minutes
'Blockage'
Dh31
AMPs
AMPs
IMD
IMD
IMD
AMPs
t+6 hours
'Killing'
AMPs
AMPs
AMPs
AMPs
AMPs
AMPs
AMPs
AMPs

# SUPP1

**A**

ctrl + *Ecc*

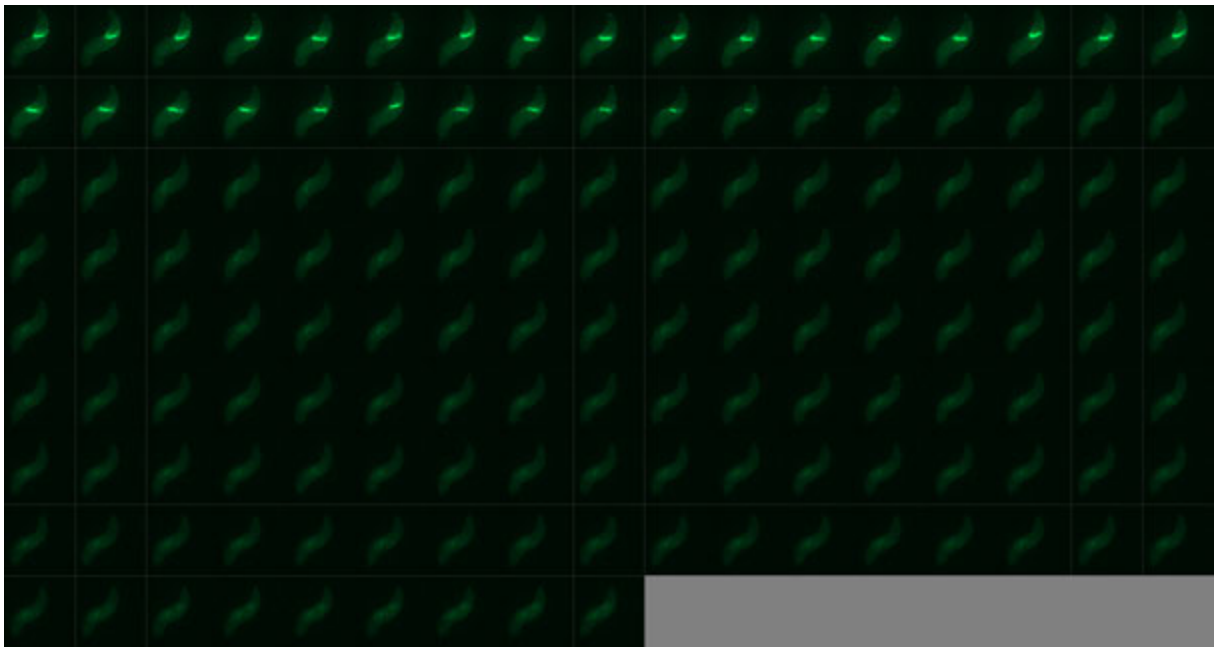

**B**

ctrl + *Bt*

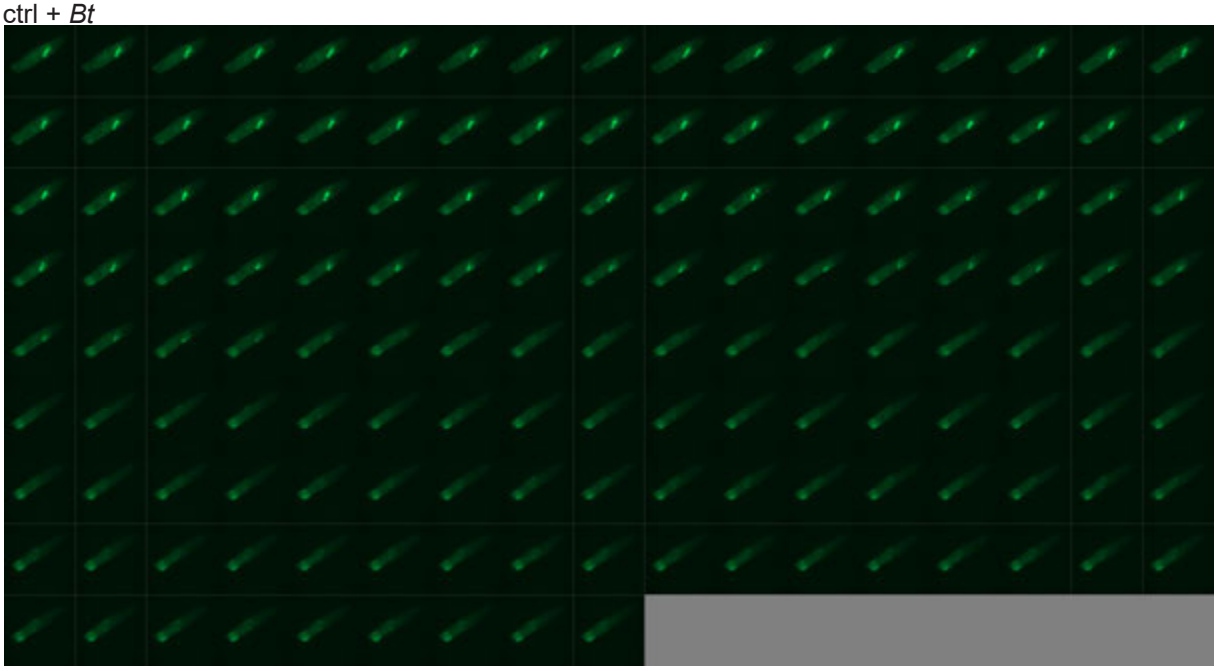

**C**

ctrl + *Lp*

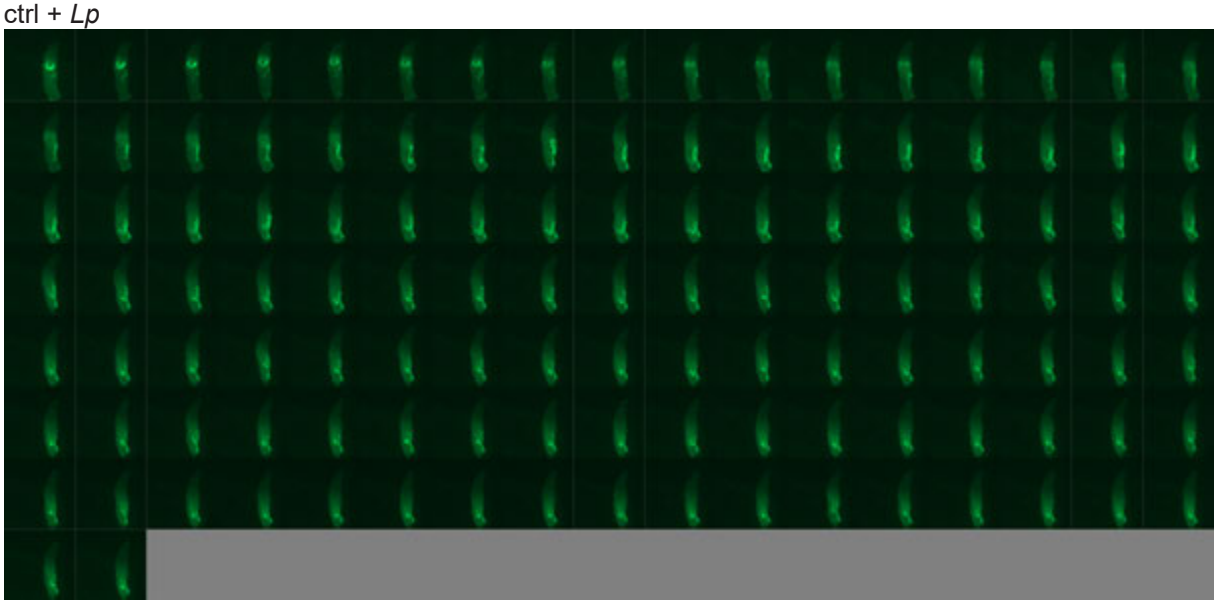

# SUPP2

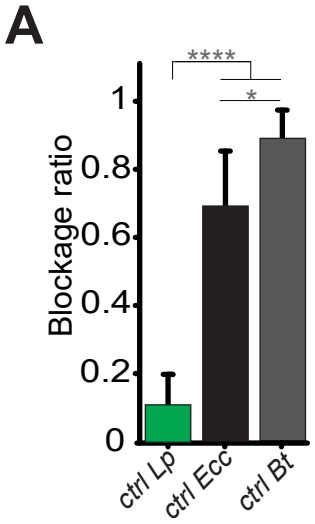

# SUPP3

**A**

*TrpA1*[1] + *Ecc*

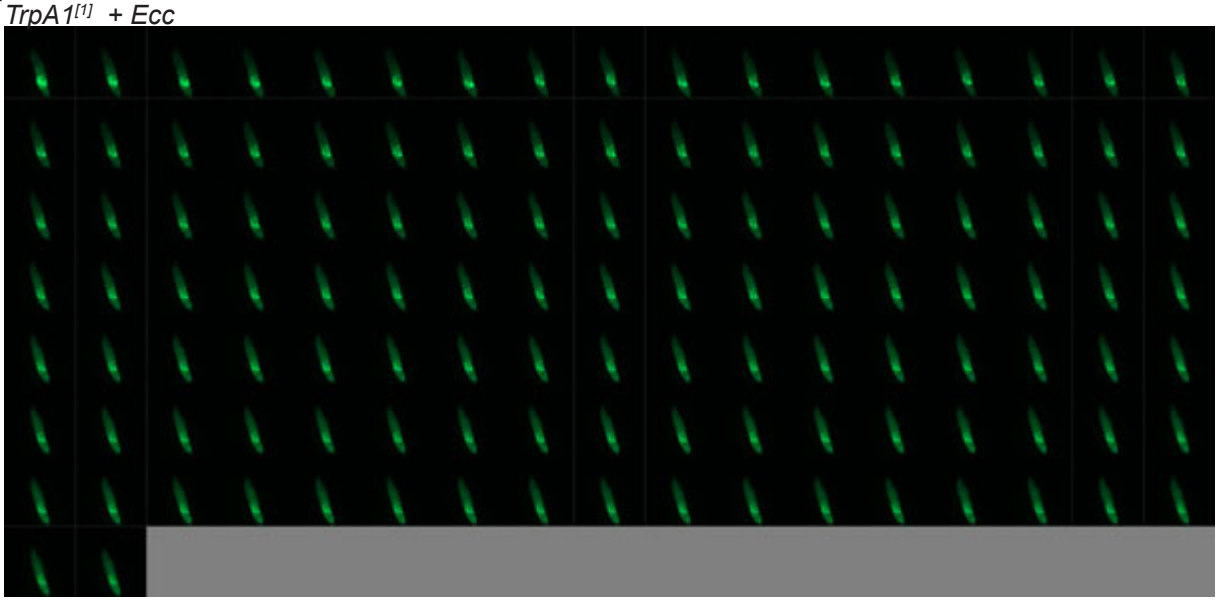

**B**

*Dh31*⁻ + *Ecc*

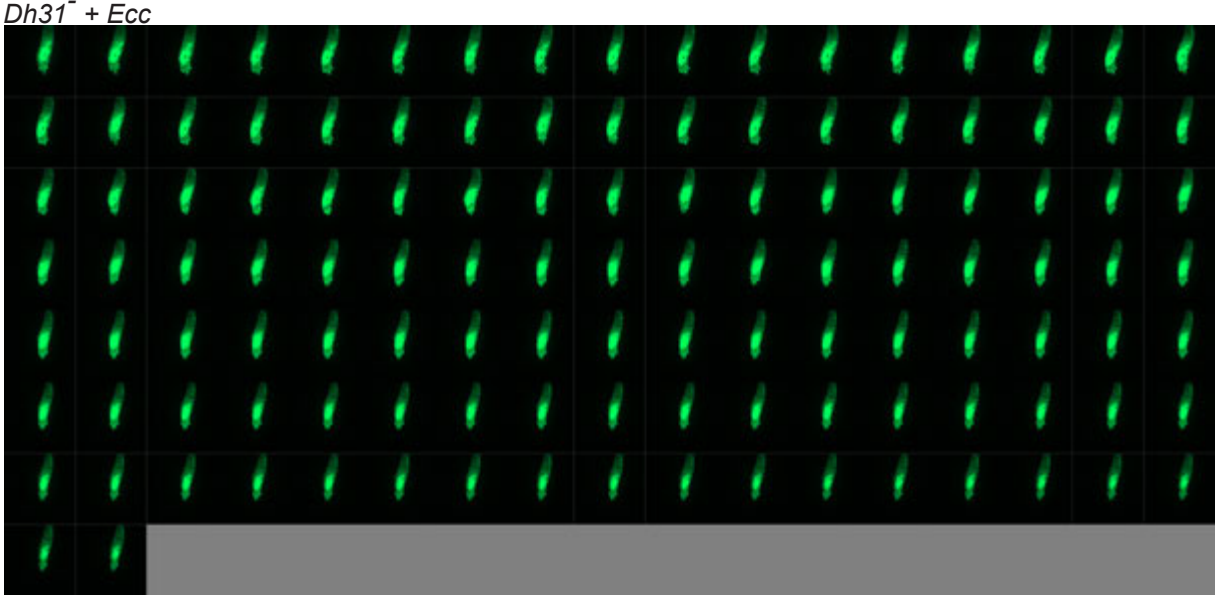

**C**

ctrl + *Lp* + hCGRP

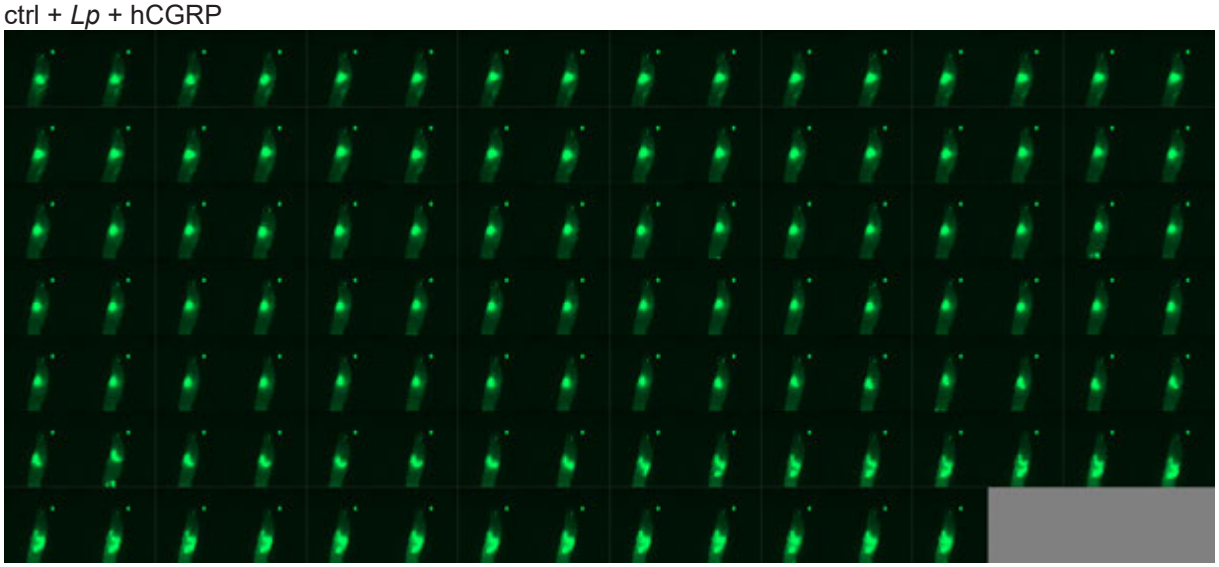

# SUPP4

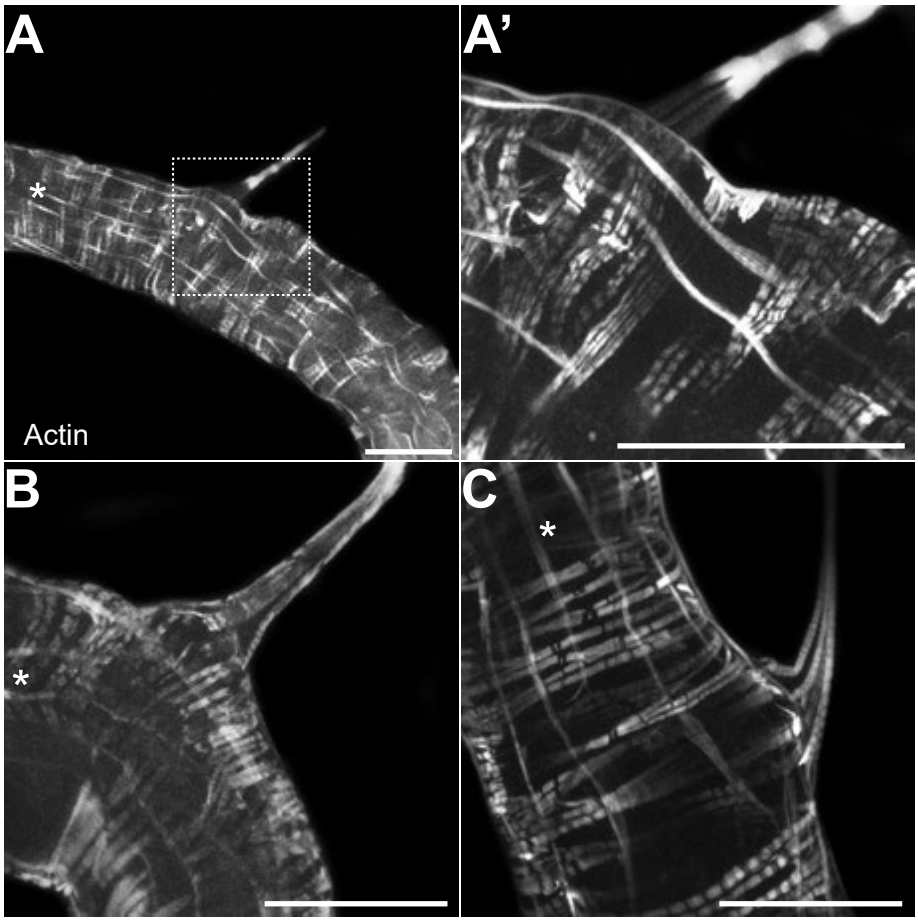

# SUPP5

**A** *PGRP-LC[ΔE] Bt*

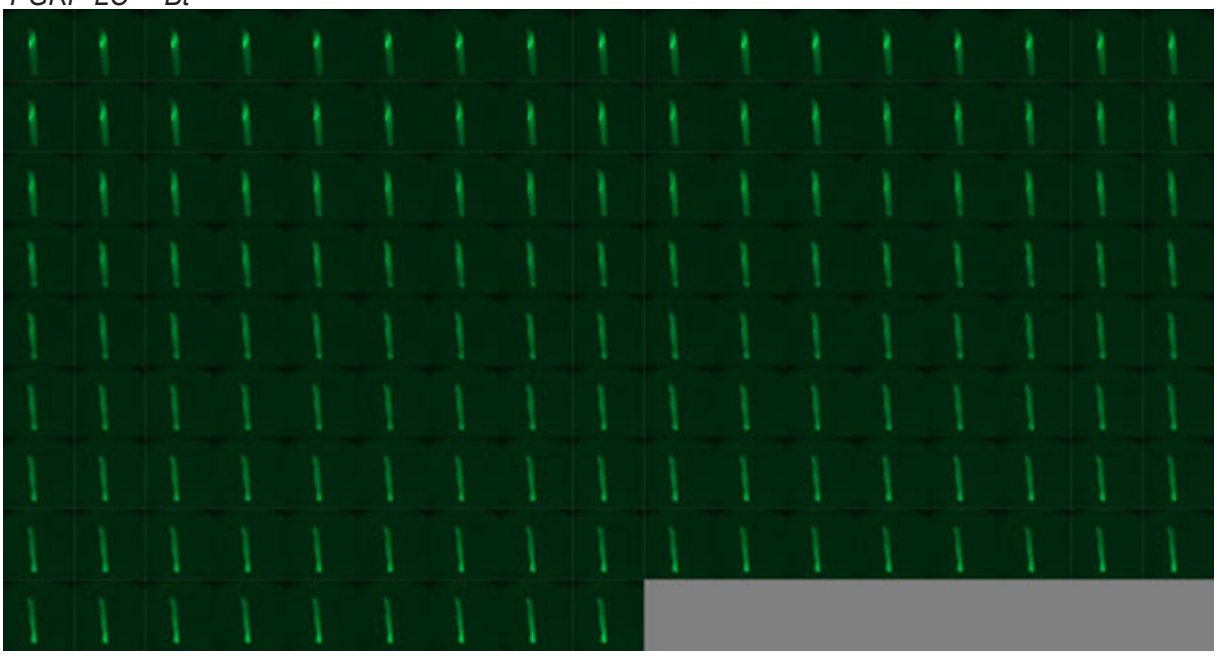

**B** *PGRP-LE[112] Ecc*

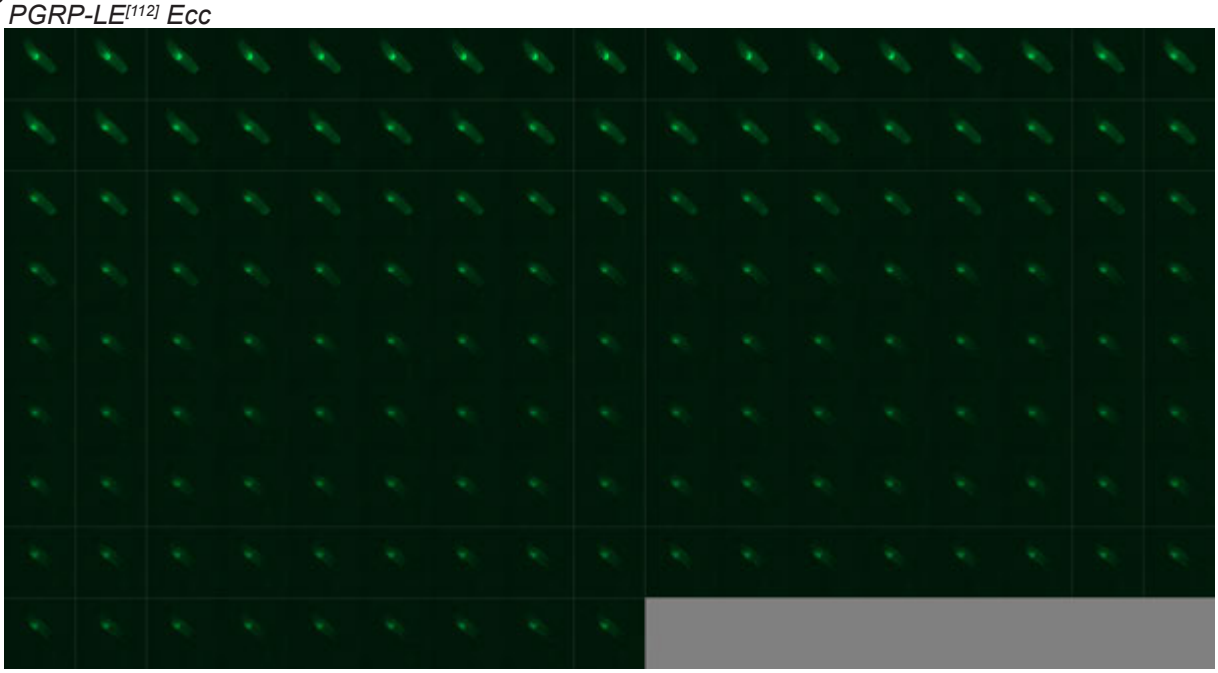

SUPP6

**A** *Dredd*[F64] *Ecc*

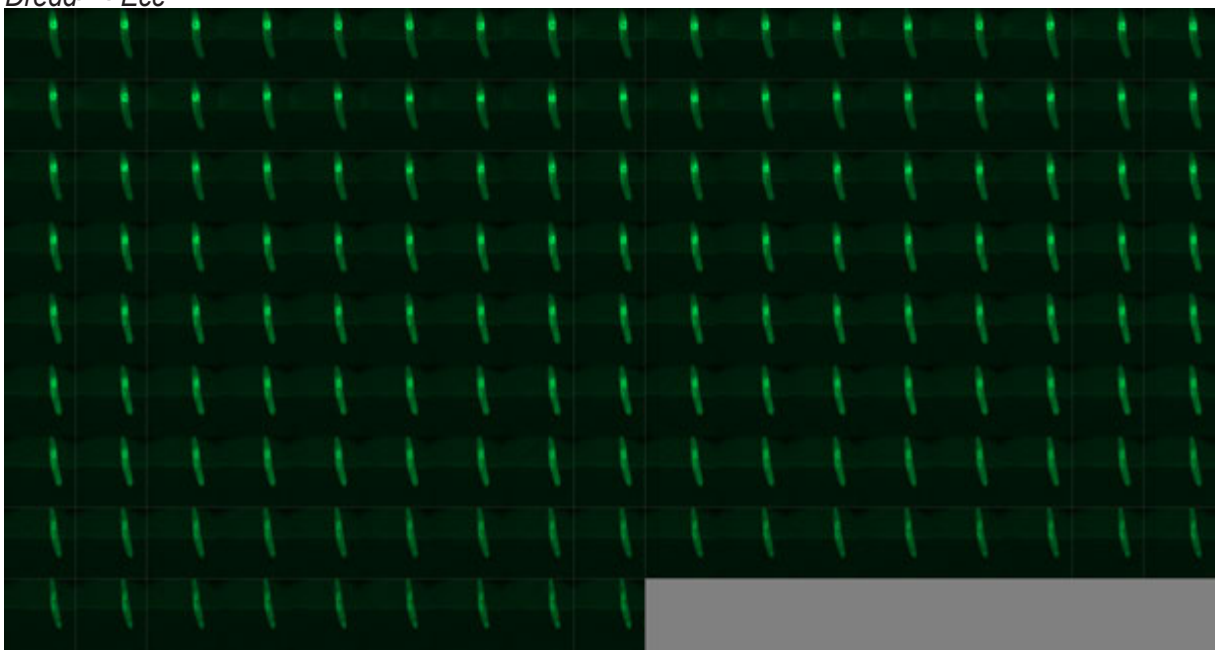

**B** *Rel*[E20] *Bt*

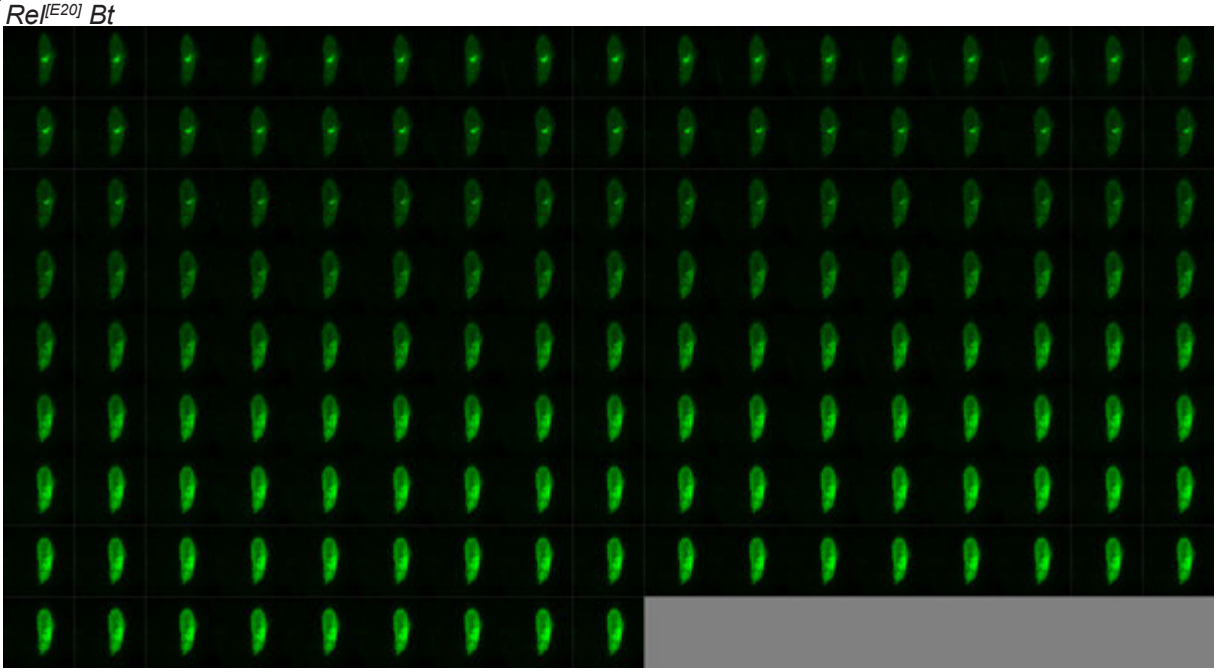
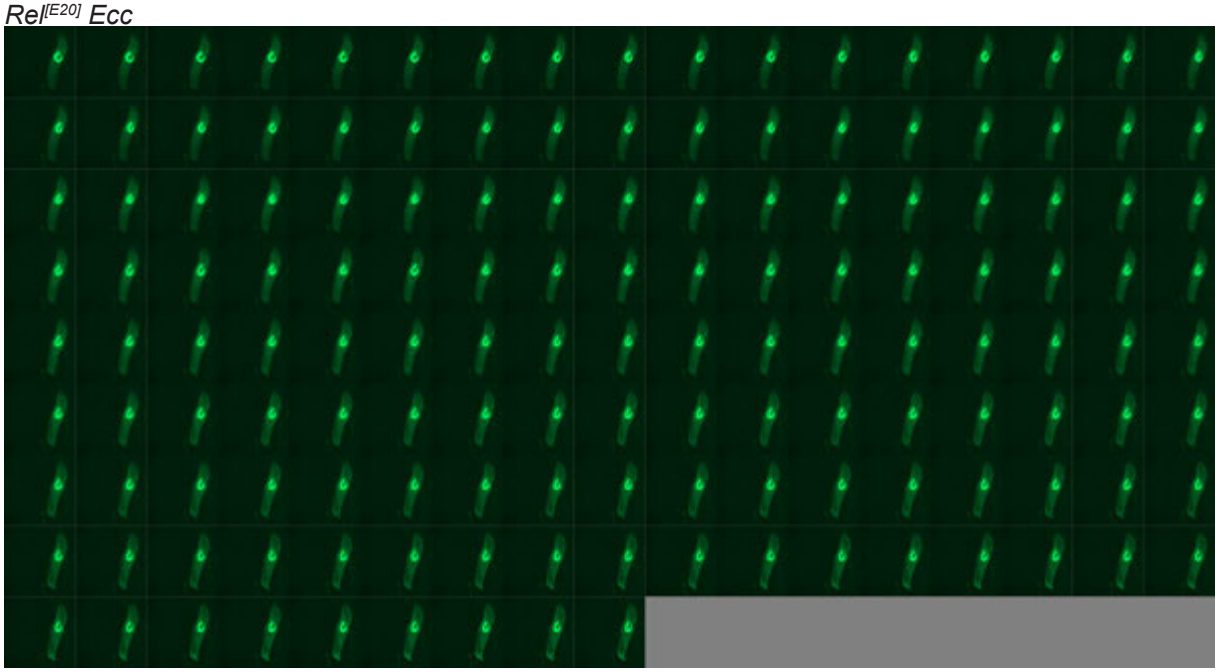
**C** *Rel*[E20] *Ecc*